TRIIN KANGUR

Preparation and functional properties of stochastic microstructured sol-gel silica materials

TARTU ÜLIKOOL
UNIVERSITAS TARTUENSIS
1632

DISSERTATIONES SCIENTIAE MATERIALIS UNIVERSITATIS TARTUENSIS

23

TRIIN KANGUR

Preparation and functional properties of stochastic microstructured sol-gel silica materials

The study was carried out at the Institute of Physics, Department of Material Science, Faculty of Science and Technology, University of Tartu.

The Dissertation was admitted on December 5, 2017 in partial fulfilment of the requirements for the degree of Doctor of Philosophy in Material Science and allowed for defense by Scientific Council on Material Science of the Faculty of Science and Technology, University of Tartu.

Supervisors: Dr. Martin Järvekülg, Institute of Physics, University of Tartu
                Dr. Valter Kiisk, Institute of Physics, University of Tartu
                Dr. Ants Lõhmus, Institute of Physics, University of Tartu

Opponents: Dr. Janis Locs, Riga Technical University
                Prof. Urve Kallavus, Tallinn University of Technology

Defense: February 12, 2018, at University of Tartu, Estonia

European Union
European Regional
Development Fund

Investing
in your future

CONTENTS

LIST OF PUBLICATIONS

I.   **T. Kangur**, V. Kiisk, A. Loot, M. Timusk, M. Järvekülg, Optical functionality of micro- and nanostructured silica surfaces prepared by a sol-gel phase separation method, *Thin Solid Films* 622 (2017) 11–16.

II.   **T. Kangur**, L. Nurmis, M. Järvekülg, Influence of some system parameters on silica surface patterns by sol-gel phase separation method, *IOP Conference Series: Materials Science and Engineering* 49 (2013) 012035.

III.   P. Reemann, **T. Kangur**, M. Pook, M. Paalo, L. Nurmis, I. Kink, O. Porosaar, K. Kingo, E. Vasar, S. Kõks, V. Jaks, M. Järvekülg, Fibroblast growth on micro- and nanopatterned surfaces prepared by a novel sol-gel phase separation method, *Journal of Materials Science: Materials in Medicine* 24 (2013) 783–792.

IV.   M. Timusk, A. Kuus, K. Utt, **T. Kangur**, A. Šutka, M. Järvekülg, M. Knite, Thick silica foam films through combined catalytic decomposition of H_2O_2 and sol-gel processes, *Materials and Design* 111 (2016) 80–87.

Author's contribution

Paper I: Elaboration of synthesis protocols and preparation of samples. Characterization of surface morphology, influence of synthesis parameters and wetting properties. Participation in optical characterization. Writing the main part of the manuscript.

Paper II: Elaboration of synthesis protocols and sample preparation. Characterization of the prepared coatings. Writing the main part of the manuscript.

Paper III: Participation in creating of bibliographical background. Preparation and characterization of cell growth substrates. Writing of the experimental part of the manuscript related to the patterned substrates.

Paper IV: Participation in morphological characterization and analysis of the sample and in manuscript preparation.

OTHER PUBLICATIONS OF THE DISSERTANT

I.   M. Klaas, **T. Kangur**, J. Viil, K. Mäemets-Allas, A. Minajeva, K. Vadi, M. Antsov, N. Lapidus, M. Järvekülg, V. Jaks, The alterations in the extracellular matrix composition guide the repair of damaged liver tissue, *Scientific Reports* 6 (2016) 27398.

II. K. Siimon, P. Reemann, A. Põder, M. Pook**, T. Kangur**, K. Kingo, V. Jaks, U. Mäeorg, M. Järvekülg, Effect of glucose content on thermally cross-linked fibrous gelatin scaffolds for tissue engineering, *Materials Science and Engineering C* 42 (2014) 538−545.

III. M. Järvekülg, R. Välbe, J. Jõgi, A. Salundi, **T. Kangur**, V. Reedo, J. Kalda, U. Mäeorg, A. Lõhmus, A.E. Romanov, A sol-gel approach to self-formation of microtubular structures from metal alkoxide gel films, *Physica Status Solidi A – Applications and Materials Science* 209 (2012) 2481−2486.

IV. V. Kiisk, **T. Kangur**, M. Paalo, T. Tätte, S. Lange, S. Pikker, I. Sildos, Structural and luminescence characteristics of SnO_2:Eu and SnO_2:Eu,Sb nanophosphors upon annealing at high temperatures, *Materials Chemistry and Physics* 130 (2011) 293–298.

ABBREVIATIONS

AFM	atomic force microscope
AR	antireflection
FIB	focused ion beam
RH	relative humidity
SEM	scanning electron microscope
TEOS	tetraethyl orthosilicate
TMOS	tetramethyl orthosilicate
WCA	water contact angle
Vis-NIR	visible and near-infrared (spectral range)

1 INTRODUCTION

Our current and future technologies require materials with a wide range of specific functions. Among other properties, the morphology can be critical in defining the functionality of a material. Sol-gel is a versatile technology which enables to prepare materials in various shapes and sizes. In terms of applicability, methods that can be scaled up to industrial scale are superior in the production of a material. Compared to frequently applied top-down lithography methods, the low-cost and bottom-up nature of sol-gel processing is advantageous for the industrial scale-up. Hydrolytic sol-gel processes have great potential in the preparation of different oxide materials, including silica. Silica is found abundantly in nature, it has been extensively studied in the field of nanotechnology and materials science in general, and is widely used in everyday life.

The primary object of this study was surface patterning of novel silica coatings, consisting of round-shaped silica microstructures. We can foresee at least three application areas for such structured surfaces. First, the mild preparation processes that enable functionalization with organic groups, bio-polymers or -molecules make sol-gel method attractive for biomaterial and biointerface research. It is shown in literature that cell functions can be affected by substrate topography. Second, the round surface structures bear a resemblance to miniature microlenses and therefore have non-trivial optical properties. In this work, antireflection and light trapping properties were addressed. In addition, surface structuring can provide the material special wetting properties that can lead to applications as self-cleaning coating. Moreover, in the case of self-cleaning windows, the optical and wetting properties of surfaces are a simultaneous concern.

The second object of the study was a macroporous silica foam film prepared by sol-gel method. Porous ceramics are good high-temperature thermal insulation materials. For example, oxide aerogel materials are widely studied due to their extremely low density and thermal conductivity, but unfortunately most of the preparation methods are time consuming and costly.

Although material preparation by sol-gel is in general relatively fast and facile, numerous parameters influence the final product of sol-gel synthesis. The primary purpose of this research was to clarify the influence of preparation system parameters on the round silica surface structures and silica foam films, and also, bearing in mind the applications mentioned above, to evaluate the applicability of these coatings in different fields. Morphology of these coatings is formed through template-free system, where structure formation is based on concurrent phase separation and sol-gel transition processes. The structured surfaces with randomly positioned domes have a potential to realize single-layer multifunctional coatings combining self-cleaning and light-scattering or -collecting properties. The foams presented in this thesis can be good alternatives to aerogel-like thermal insulation materials.

2 AIMS OF THE STUDY

The aim of present work was to develop sol-gel approaches for preparing silica materials with characteristic micro-morphological features and evaluate their potential in some application fields. In particular, we aimed to develop methods and prepare samples of surface coatings of silica domes and silica foams and carry out the preliminary characterization of their critical functional properties in corresponding applications. The preparation and properties of the silica foams are covered briefly whereas the main focus is on the structured coatings via sol-gel phase separation method.

Three specific goals were set:

1. to provide, based on experimental observations, description of the sol-gel processes leading to the formation of the silica materials with the round-shaped structuring;
2. to clarify the influence of synthesis parameters on the morphology of the prepared structures and optimize the synthesis accordingly;
3. to evaluate the potential of the obtained materials in various applications: structured silica surface as cell growth substrate and optically functional material, and silica foam as thermal insulation material.

3 BACKGROUND

3.1 Sol-gel method

3.1.1 Introduction

Sol-gel method is a versatile technology, which enables to prepare ceramic powders, fibers, films, microrolls and -tubes, template-based materials and aerogels [1–4]. Also, it allows tuning of nano- and microstructure, chemical composition as well as mechanical properties and functionality of materials. Some of the main advantages of material preparation by sol-gel technology are the low-temperature synthesis under mild conditions and possibility to dope and chemically functionalize these oxide materials with different elements and organic groups rather easily [2, 5]. Sol-gel materials are often applicable as sensors [6], catalysts [7], protective coatings [8], optical coatings [9], biomaterials [10] etc.

In the University of Tartu, Institute of Physics the following sol-gel materials have been prepared and studied: oxide tips for scanning probe microscopy [11]; photoluminescent films and powders [2, 12]; rare earths doped Ti- and Zr-oxide sensor materials [13, 14]; Zr- and Hf-oxide microrolls [15]; Zr-oxide microtubes [16]; Si-oxide nanotubes [17]. Also, based on phase separation in sol-gel system, electro-optical films with variable transmittance have been prepared [18].

3.1.2 Sol-gel processes

Sol-gel processes proceed through different paths depending on whether the precursor is metal or silicon alkoxide. The term sol-gel is also used in case of halide precursors and other compound systems where the underlying chemistry can be significantly different. As in present thesis the materials are prepared only from silicon alkoxides (TEOS, TMOS), only the related sol-gel processes are described here.

Historically first studied and also most widely used sol-gel processes are of silicon alkoxides. Generally, sol-gel chemistry of alkoxides consists of hydrolysis and polycondensation reactions [19–21]. These reactions are strongly influenced by water to alkoxide molar ratio and type of alkoxy groups as they can impact hydrolysis rates. Additionally, type and amount of solvent influence the reaction processes as well as reaction temperature and surrounding humidity. Solvent is needed to enhance mixing or to direct interaction of solvent molecules with silicon center. Surrounding humidity becomes important when structure forming takes place in ambient environment. Type and concentration of catalyst are also very important process parameters. Acid or base catalyst is used as silicon alkoxide reactions would otherwise result in very slow gelation rates and the catalyst concentration influences the rate of hydrolysis and

polymerization. Schemes of hydrolysis and condensation reactions with either acid or base catalyst are presented in figure 1.
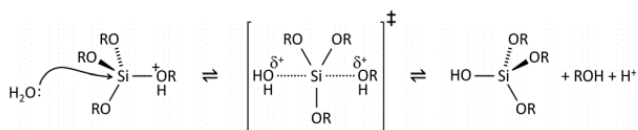
Scheme 1 Acid catalysed hydrolysis of silicon alkoxides.
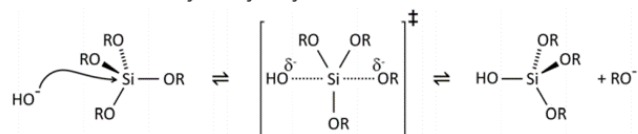
Scheme 2 Base catalysed hydrolysis of silicon alkoxides.

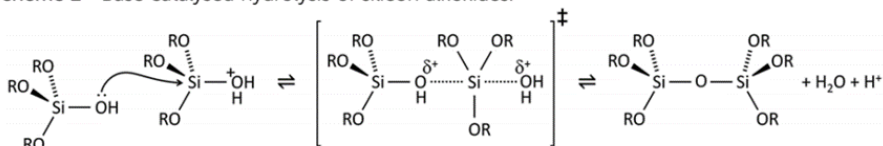**Scheme 3** Acid catalysed condensation of silicon alkoxides.
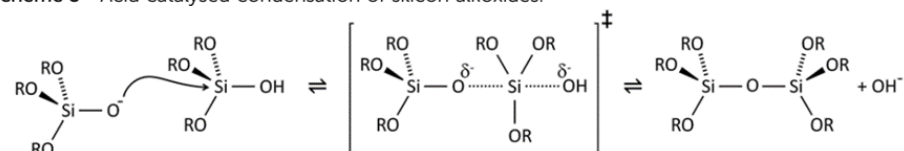
Scheme 4 Base catalysed condensation of silicon alkoxides.

Figure 1. Schemes for hydrolysis and condensation reactions of silicon alkoxides [21].

The first step is hydrolysis of alkoxide, which is followed by the condensation reactions resulting in –Si–O–Si– linkage. Reactions in figure 1 are simplified and in reality these reactions can undergo parallel, however hydrolysis is necessary for the condensation to occur [22]. The structure of the resulting gel is different depending on the catalyst type (Fig. 2) [21]. Continuous hydrolysis steps get progressively slower under acidic conditions and faster under basic conditions. In basic conditions hydrolysis is complete before the first condensation step occurs and it results in small and branched agglomerates in the sol, which eventually crosslink to form a colloidal gel. In acidic conditions the hydrolysis step is typically the fastest and condensation begins before hydrolysis is complete. This results in the formation of chain-like structures in the sol and finally a network-like gel. The structures studied in this thesis are formed through acid catalyzed reactions.
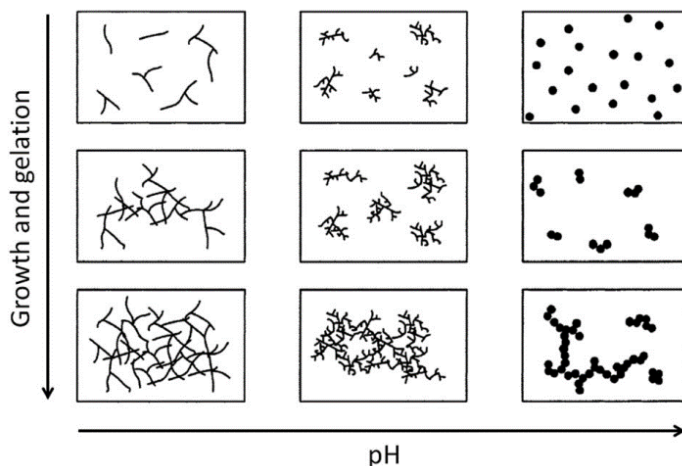
Figure 2. Diagram showing how pH affects the growth and structure of a gel [21].

Cross-linking induces an increase of viscosity of the sol and this leads to gelling of the solution. A three-dimensional network is formed. Solvent evaporation results in xerogel which is formed when drying with unhindered shrinkage. Final drying at room temperature or elevated temperatures results in an amorphous or crystalline oxide material.

Formation of silica domes presented in this thesis is based on sol-gel phase separation processes. The phase separation mechanism has been typically used for preparing porous materials [23]. However, formation of silica domes can also be related to the sol-gel phase separation mechanisms greatly studied by K. Nakanishi et al. (first systematic study in 1991 [24]), described in the following chapter.

3.1.3 Phase separation

Conventional sol-gel phase separation method enables to prepare porous oxide materials with different morphologies and porosities [22–27]. The general nature of mechanisms behind formation of these kinds of morphologies can be explained based on the chemical polymerization reactions.

Relatively narrow distribution of growing oligomers is obtained, when acidic conditions are applied for hydrolysis and polycondensation of alkoxysilanes. The average molecular weight of the polymerizing species increases and the mutual solubility between the constituents becomes lower and separation of phases imposes a decrease of entropy. This leads to an increase of the free energy of mixing described by the following equation:

$$\Delta G = \Delta H - T\Delta S, \tag{1}$$

where ΔH is change in the enthalpy of mixing, $T\Delta S$ is the entropy of mixing. ΔG is negative in case of miscibility. If the ΔG becomes positive as the result of decreased absolute value of the $T\Delta S$, a thermodynamic driving force for phase separation is generated.

Figure 3 shows a phase diagram presentation of how phase separation can be generated. In the case of physical cooling a reduction of temperature decreases the mutual solubility and results in demixing. In the case of chemical cooling the polymerization induces a reduction of the mutual solubility.
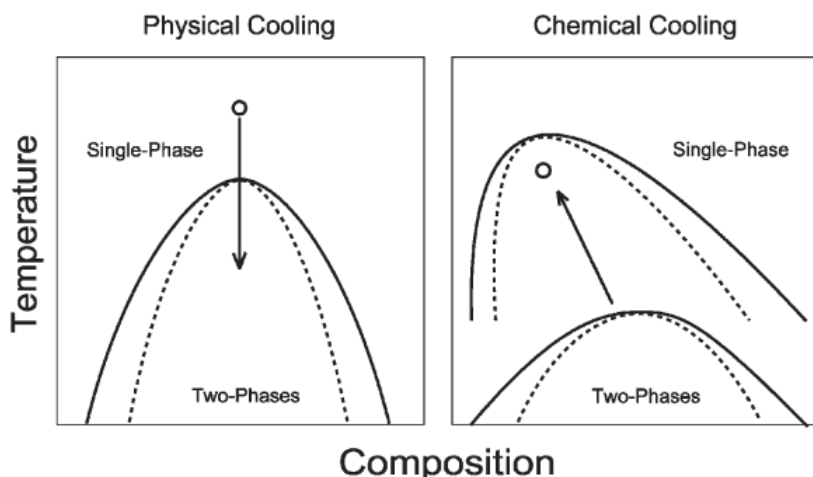
Figure 3. Comparison between physical and chemical cooling. The solid and broken boundaries respectively denote bimodal and spinodal lines. [22]

The two-phase area between broken boundaries is the unstable region (Fig. 3), where the spinodal decomposition occurs resulting in a bicontinuous morphology (Fig. 4). Spinodal decomposition leads to development of a co-continuous structure, but it might not be permanent. Characteristic size of the domains can be changing in time until fragmentation occurs which leads to a system, where the domains of one phase are dispersed in another continuous phase (Fig. 4). Analogous fragmentation can also occur through nucleation and growth mechanism. This mechanism occurs in the metastable region between the bimodal and spinodal lines and it can be initiated by two reasons: by thermally induced microscopic composition fluctuation or by impurities or other inclusions. The formed dispersed domains grow as additional atoms or molecules subsequently diffuse toward the nuclei. The latter mechanism is proposed to be the one that is involved in the formation of the silica domes presented in this thesis.
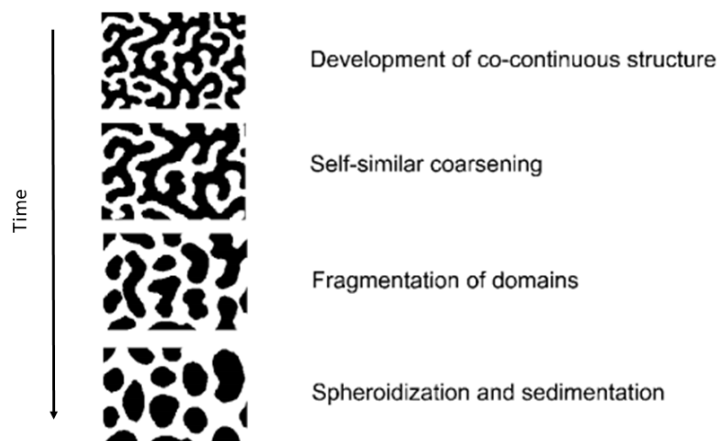
Figure 4. Time evolution of a spinodal decomposing [25].

Final structure is formed, when one phase turns from a viscous fluid to an elastic solid as structure freezing by irreversible sol-gel transition is occurring. It is initiated by polycondensation reactions of network-forming siloxane species. The final structure depends on the onset of phase separation relative to the sol-gel transition point. The longer the time gap is between these two processes, the coarser the final morphology is (or eventually fragmentation occurs). The size of phase-separated structures can be controlled by the same parameters which affect the sol-gel reactions.

3.2 Functional microstructured coatings

3.2.1 Optical functionality

Antireflection and light trapping are important qualities for applications like solar cells, photodetectors and optical surfaces [28–30] and an approach to achieve these qualities is provided by various kinds of surface structuring like pyramidal texturing [31], black silicon [32], moth-eye structures [33] and microlens [34] (Fig 5) etc. For example, improvement of absorption of incident light is needed to enhance photoconversion efficiency in solar cells [35–37].

Biomimetic approaches have become increasingly popular for designing optically functional materials [38]. For example, moth-eye structuring representing broadband antireflection is a good example from nature [33, 39]. Moth-eye structuring means that there is a regular array of small bumps covering the surface, whereas the spacing and size of the bumps are comparable to the wavelength of light [40] (Fig 5a). Antireflection is also exhibited with porous or irregular surface structures [41, 42]. Random structuring may even lead to a better overall performance compared to a regular array of structures [33, 43] (Fig 5b).
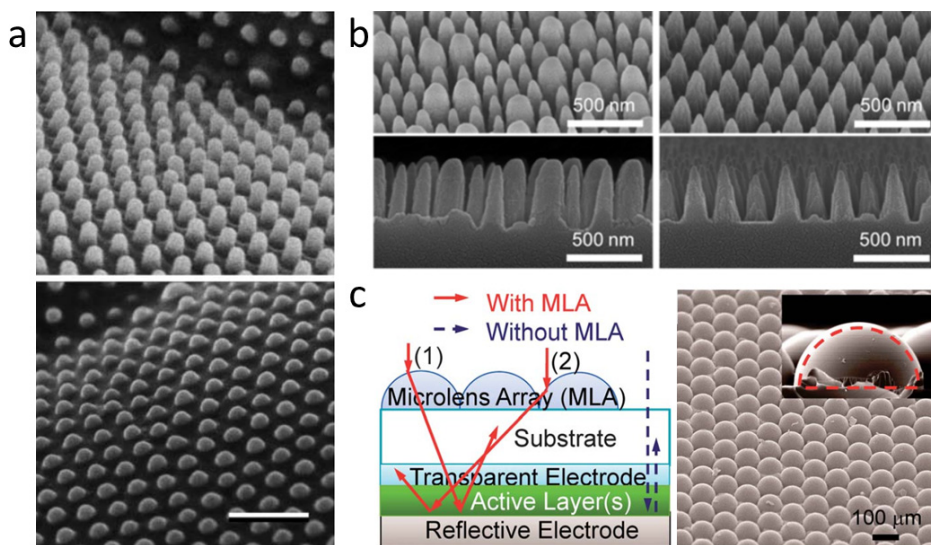
Figure 5. a) SEM images of different moth-eye structuring of corneal nipple arrays in two butterflies (the scale bar is 500 nm) [44]. b) SEM images of moth-eye mimicking random and periodic arrays [33]. c) Schematic illustration of light behavior with and without a microlens array (MLA) for a conventional organic photovoltaic device and SEM image of representative MLA [34].

Some results of silica-based optically functional materials obtained via sol-gel technology have been already demonstrated. Manca et al. presented durable transparent antireflective coating from trimethylsilanized silica nanoparticles embedded in organosilica gel matrix [45]. Xiu et al. created a rough silica film with superhydrophobic properties with the help of templating agent [46]. In addition, rough silica surfaces are suitable to reduce reflections from glass surfaces of optical elements and windows [47, 48], where specular transmittance may or may not be needed, depending on the application.

3.2.2 Water-repellency and surface roughness

Surface roughness is a one of the key factors determining surface wettability. Water-repellent plants, for example Lotus, are known to have self-cleaning properties, and developing superhydrophobic surfaces which mimic Lotus leaf have been widely reported in literature [49–51]. Surface is considered to be superhydrophobic when static water contact angle (WCA) is larger than 150° [51]. Exact mimicry of Lotus leaf implies dual-scale surface roughness, where microbumps are covered with additional nanoscale structuring (Fig. 6). Water droplet sits on the apex of nanostructures which minimizes the contact between the surface and the droplet (Fig. 7). Also, extremely small sliding angle is very

important property for water-repellent and self-cleaning surfaces. It means that water droplets need to roll-off from the surface at minimal tilt, not sticking to it. For a great performance the sliding angle should be 5° or smaller [52]. High air ratio at the interface between solid and water is important for obtaining a small sliding angle [53].
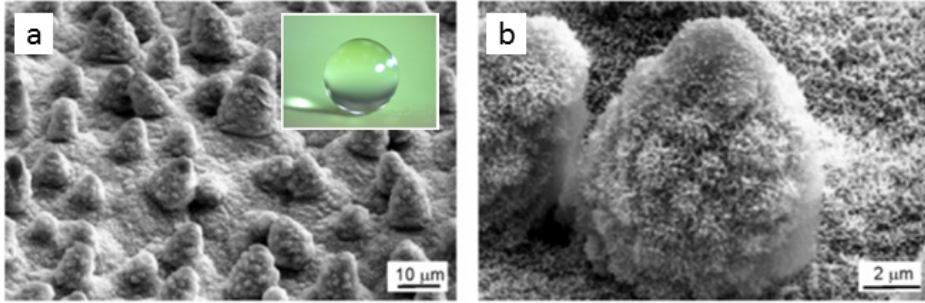
Figure 6. SEM micrographs of Lotus leaf surface at two magnifications (a, b). Inset of a) shows water droplet sitting on the Lotus leaf [50].
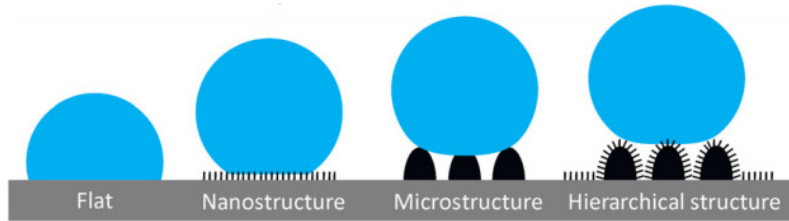
Figure 7. Schematic of wetting of four different surfaces. The contact area between the droplet and the surface is the largest in the case of flat and microstructured surfaces, but is reduced on nanostructured surfaces and is minimized on hierarchically structured surfaces [50].

There are different models describing wetting behavior on different surfaces [51, 53–56]. Wetting models are based on the ideal flat surface described by the Young's equation:

$$cos(\theta_Y) = \frac{\gamma_{sg} - \gamma_{sl}}{\gamma_{lg}} \tag{2}$$

where γ_{sg}, γ_{sl} and γ_{lg} are surface tensions at solid-gas, solid-liquid and liquid-gas interfaces, respectively. In reality, there are no ideally flat surfaces. Wenzel took the surface roughness into account while assuming that the liquid fills the

protrusions on the rough surface (Fig. 8a). It is also called homogeneous wetting state. This modification can be described with the following equation:

$$\cos(\theta_W) = r \cos(\theta_Y) \qquad (3)$$

where θ_W and θ_Y are Wenzel's and Young's contact angles and r is the roughness factor defined as the ratio of the actual area of a rough surface to the geometric projected area. Heterogeneous wetting state describes the surface as a two-material system, where one of the materials is trapped air between protrusions and water droplet contacts only the top of protrusions (Fig. 8b). This system is described by Cassie-Baxter's equation:

$$\cos(\theta_{CB}) = r_f f \cos(\theta_Y) + f - 1 \qquad (4)$$

where f is the contact area between water droplet and solid surface and r_f is the roughness factor of the wet area. However, these models are not sufficient to describe the real situations as there might be cases, where both approaches need to be considered, especially for multilayered or complex roughness (Fig. 8c). The latter makes the evaluation of accurate roughness factor complicated in real situations, therefore, in the present thesis these formulae are not applied.
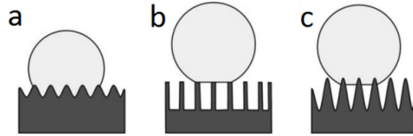
Figure 8. Wetting states of Wenzel (a), Cassie–Baxter (b) and combined models (c) [51].

3.2.3 Structured biointerfaces

Cells have highly complex and dynamic interaction with surrounding environment – extracellular matrix (ECM) and other cells. ECM plays an essential role in cell growth processes – migration, differentiation and proliferation [57]. Previous studies have shown that cell behavior can be influenced and possibly directed by modifying properties of the environment surrounding the cells. The topography has important role in cell adhesion, shape and movement [58, 59]. Cell growth is affected by the mechanical properties [60], surface chemistry [61], micro- and nanostructure [62, 63] of the surrounding environment. Additionally, materials' electrical properties are significant as electrical stimulation has been shown to enhance wound healing [64]. Therefore, materials science aims at the development of artificial materials (substrates, matrixes, scaffolds, etc.) that would enable the elaboration of artificial tissue scaffolds which would match the environment experienced by cells in living tissues.

Structural biofunctionality is represented in this dissertation. Structured silica substrate with round surface features is a more biomimetic approach compared to the sharp and edged nano- and micropatterns prepared by conventional lithographic methods [65]. Sol-gel silica materials have been shown to be biocompatible [66], in some cases also biodegradable [67] and to enhance differentiation and proliferation of cells [68]. Silica-based sol-gel glasses have also been shown as good bioactive glasses [69, 70]. An additional advantage is that the sol-gel processes allow preparation of the silica-based glass materials in various forms and shapes, such as coatings [71], fibers [72], foams [73], nano- and microparticles [70, 74]. Especially surface coatings are of interest as they can enhance biocompatibility for biomedical devices and promote the healing response without causing any rejection reactions [75]. For example, silica-based materials are widely applied in bone tissue engineering field [10, 70].

3.2.4 Porous oxide structures

Sol-gel technology together with various fields of research have been applied to synthesize oxide foams. These materials find applications in catalysis [76], electrochromic devices [77], high performance thermal insulation [78], chromatography columns [25] and also biomedical materials [73]. As mentioned in the sol-gel section (Ch. 3.1.3) porous oxide structures can be prepared along with sol-gel phase separation processes. Bimodal pore structures are formed in different morphologies from aggregates of nano- and microparticles to macro-porous monoliths [26, 79, 80]. Emulsion templating have also led to methods for preparing macroporous oxide foams [81]. In that case there are immiscible emulsion droplets in continuous alkoxide solution, which can be removed by evaporation or dissolution after gel forming around these droplets [82–84]. Different metal alkoxides allow to produce a wide variety of porous materials. Furthermore, porosity can also be formed in the presence of surfactant by bubbling the gas through matrix [85] or with an intense mechanical agitation [86]. Alternatively, the gas phase may also be created by evaporating a low boiling point component from the sol [87]. However, in situ gas phase generation would be the most attractive approach. With this aim, Chandrappa et al. introduced the vanadium oxide foam formation with decomposition of hydrogen peroxide [88]. The only work reporting pore forming through H_2O_2 decomposition similarly to the method presented in present work has been carried out by Vuong et al. [89], but their work is severely lacking as there is no information about silica precursor or thorough description about the structure forming.

4 PREPARATION AND FORMATION PROCESSES OF SILICA MICROSTRUCTURES

4.1 Silica domes [Papers I, II, III]

Structured coatings were prepared by spin-coating or spraying a sol of TEOS in alcohol (1-propanol, ethanol, or methanol) using nitric acid as catalyst (Fig. 9). All chemicals were purchased from Sigma-Aldrich. The mixing of chemicals was carried out by using a magnetic stirrer at room temperature. The first step was dilution of TEOS in alcohol, whereas the alcohol-TEOS volume ratio (T) was varied for different concentrations from 1 to 30. Secondly, for hydrolysis and condensation reactions, the acid in water was added dropwise to alkoxide solution. For varying water-alkoxide molar ratio (R) and acid-alkoxide molar ratio (K), different amounts of water (deionized water) and nitric acid were added. R was varied from 0.5 to 4 and K from 0.05 to 0.2. Finally, the solution was left stirring for 3 hours before spin-coating or spraying. The substrates (soda-lime glass microscope slides) were cleaned with methanol and hydrochloric acid solution (1:1) for 30 minutes followed by methanol rinse in ultrasonic bath and drying in nitrogen flow.
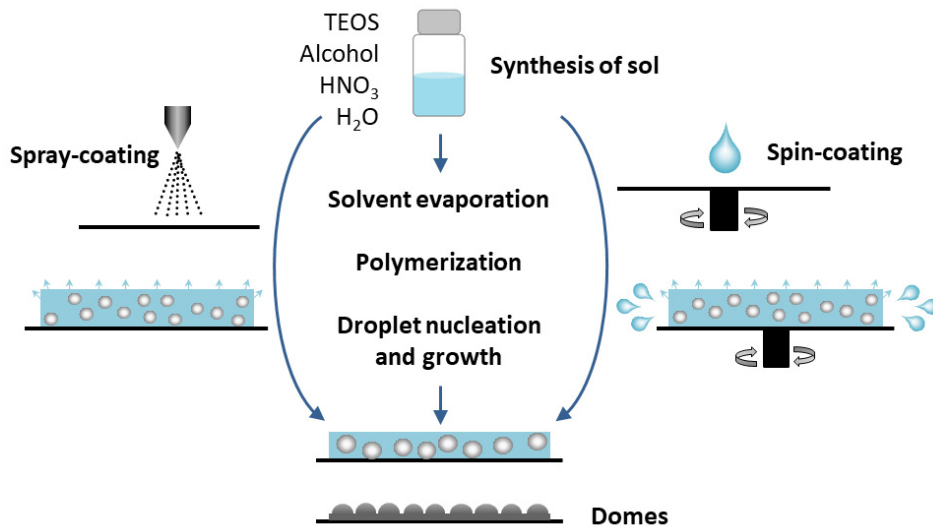
Figure 9. Scheme of structured coating formation by spray- and spin-coating.

For spin-coating a home-built machine was used at speed of 2000 rpm. The sol was dropped with a pipette onto the spinning glass substrate. For spray-coating the sols were sprayed onto the glass substrate by using vertically positioned fixed spray gun combined with a home-built trigger system and N_2 carrier gas. The following parameters were varied: amount of solution (A), needle position (size of the nozzle opening) and duration of spraying. All the coating procedures were carried out in an ambient lab environment of $23 \pm 1°C$ and 20–49% relative humidity, except when studying the influence of humidity. After coating the samples were air-dried and then heated at 200 °C for at least 1 hour.

Applying the solution to a surface, reactions with water from surrounding atmosphere and solvent evaporation initiate hydrolysis and condensation processes. As partially hydrolyzed TEOS is undergoing hydrolysis and polymerization reactions, the solubility of this compound is diminishing in solvent medium and droplets of TEOS-rich phase are nucleated inside the continuous solution phase. The formed solid droplets are growing due to subsequent polymerization, and simultaneously, the solvent is constantly evaporating. After that, the round surface structures are formed when spherical nano- and micro-scaled droplets are deformed after setting on the glass substrate. In most cases the droplets undergo partial flattening as they are not fully gelled. Also, the droplets may join to form larger domains with irregular shape by moving on substrate. The movement depends on the speed of TEOS condensation and solvent evaporation. Furthermore, sphere-like silica structures are formed under the condition where the polycondensation rate within the TEOS-rich domains is high enough (and solvent evaporation from the coated layer is slow enough compared to gelling) to produce gelled silica spheres before setting on the substrate. In addition to the domes, thin continuous SiO_2 film forms onto the substrate between the domes. However, the surface chemistry does not vary between the domes and the area between them. Also, the differently patterned silica surfaces have the same surface chemistry. It is necessary to point out that the studied case is significantly different from the phase separation in thicker layers that produces porous films [19, 22] as the deposited sol is in all of its volume affected by the vicinity of either substrate-sol or sol-air interface [90].

Spin- and spray-coating methods lead to significantly different results. During the spin-coating most of the applied solution spins off the surface. Thus, the thickness of the precursor layer in which the phase separation occurs, depends on the viscosity of the solution. Spin-coating is more sensitive to variations in precursor compositions, resulting in sharper change in the size of surface features. With spraying, the domes tend to be larger in diameter and height due to the larger thickness of precursor left on the substrate, and the amount of precursor that stays on the substrate is also less influenced by the viscosity of the precursor. During the spray-coating the total surface area of the precursor is maximized in aerosol phase, leading to significant increase in solvent evaporation and exposure to air humidity. While the solvent concentration can be adjusted so that the sol is liquid (i.e. not gelled) when it reaches the substrate, the hydrolysis and condensation of TEOS is inevitably faster and

more sensitive to ambient environment than in the case of spin-coating. Also, as the substrate is not rotated, imperfect spreading of the sol can in some cases be result in thicker and uneven precursor layers. Thus, although superior in terms of scalability, spray-coating also adds complexity to already multi-variable nature of the sol-gel phase separation. Consequently, achieving repeatability and determining clear correlations between varied parameters and obtained surface structures proved to be challenging. Nevertheless, several tendencies were observable (Ch. 5.2).

4.2 Silica foam [Paper IV]

Foams were prepared by spraying TMOS-derived and H_2O_2-containing sol onto a substrate coated with MnO_2 as a catalyst (Fig. 10). The catalyst is needed for decomposing H_2O_2 at room temperature as without catalyst it can decompose only thermally requiring a high temperature. The latter is not preferred causing an uncontrollable gelation in the sol. MnO_2 was chosen as it is known from literature to be an efficient catalyst for decomposing H_2O_2 [91]. The concentration of H_2O_2, solvent (methanol, ethanol, 1-propanol, 1-butanol, 1-pentanol), and solvent concentration were varied in order to investigate the influence of these parameters on the foam formation. Further details about variation of these parameters in numbers are given in paper IV [92], but shortly the preparation was as follows. Firstly, two solutions were prepared: HNO_3 solutions in H_2O/H_2O_2 and TMOS dilution in alcohol. Then the $H_2O/H_2O_2/HNO_3$ solution was added dropwise to the TMOS/alcohol solution under vigorous stirring. Last step was addition of the foaming agent polyethyleneoxyethanol (Tergitol NP-10) for foam stabilization. After mixing, the sols were spray-coated onto MnO_2-coated glass substrates by using a vertically positioned airbrush spray gun and N_2 carrier gas. Different amounts of the sol were sprayed to prepare films with different thicknesses followed by aging and annealing up to 600°C.

Silica foam formation is initiated by H_2O_2 decomposition on MnO_2, which results in water and O_2 formation. Water leads to further hydrolysis and accelerates the gelation. The foam is formed as these two processes occur in parallel. Sol-gel transition has to occur at the exact point so that the formed bubbles would not collapse before sol-gel freezing point. Annealing can also lead to a collapse of the macroporous structure as reported by Choi and Paek [93]. However, novel for this kind of material is the ability to maintain a closed-cell morphology even after annealing.

TMOS
Alcohol
HNO$_3$
H$_2$O
H$_2$O$_2$
surfactant

Synthesis of sol

Spray-coating

← MnO$_2$ catalyst film

**O$_2$ formation
Gelation**

O$_2$

MnO$_2$

2 H$_2$O$_2$ → 2 H$_2$O + O$_2$
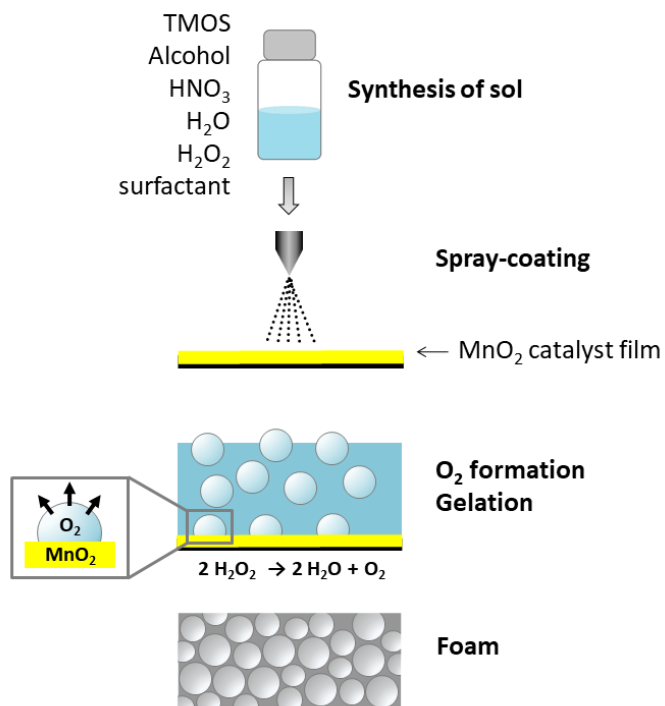
Foam

Figure 10. Scheme of silica foam formation.

5 RESULTS AND DISCUSSION

5.1 Characterization methods

The structural features of the obtained silica coatings were investigated by scanning electron microscope (SEM) analysis using FEI Helios Nanolab 600 or Tescan VEGA II SBU. The samples were tilted at 45° for a more precise view of the domes' shape. The diameters of the domes were evaluated from SEM micrographs taken at normal incidence. For electrical conductivity the samples were previously sputter coated with a 2–5 nm layer of Au/Pd alloy using a SC7640 Auto/Manual High Resolution Sputter Coater. Cross-sections of the substrates with cells were cut using focused ion beam (FIB). Optical microscope images of the foams were obtained using an Artray Artcam-500P II CCD camera mounted on an Olympus BX51 optical microscope.

For investigating the roughness and morphology of the structured surfaces, atomic force microscope images were obtained with Dimension Edge™ AFM System (Veeco Instruments Inc.) in tapping mode at room temperature. Mean roughness of the surface, height of the domes and number of domes per area were estimated by using Gwyddion software.

Diffuse reflectance spectra of the coated glass slides were measured with Cary 5000 UV-VIS-NIR spectrophotometer using an integrating sphere. Some artefacts present in the spectra were further reduced by normalizing against the known reflectance of uncoated glass slide measured for reference.

Complementary light scattering measurements were conducted on a home-built automated goniometric system in the reversed Kretchmann geometry [94] as depicted in figure 11. A laser beam was perpendicularly incident on the coated glass slide which was attached to a semicylindrical prism (using an index-matching oil). The angular dependence of the forward scattered light emerging from the prism was measured with a photodiode. Such configuration allowed a more direct assessment of the coated front surface by eliminating the reflections from the back surface. The results for *s*- and *p*-polarized light were averaged to obtain effectively the response for unpolarized light.

Water contact angles were measured with GIMP software from optical micrographs taken with a digital photo camera (Canon EO5 650D with objective Canon MP65). Samples were stored in a closed box, and rinsed with methanol and dried in compressed air before WCA measurements. WCAs were acquired from 4 µl water droplet at three different locations on each sample and the obtained values were averaged.

For imaging different parts (nuclei, cytoskeleton) of cells several staining procedures were performed [65]. Immunofluorescence microscopy was carried out with an Olympus FluoView FV1000 microscope. For counting of adhered cells (counting cells with atypical morphology) Zeiss Axiovert S100 inverted microscope was used. Data was collected from four randomly chosen fields from four cover slips. Images were analyzed with ImageJ software.
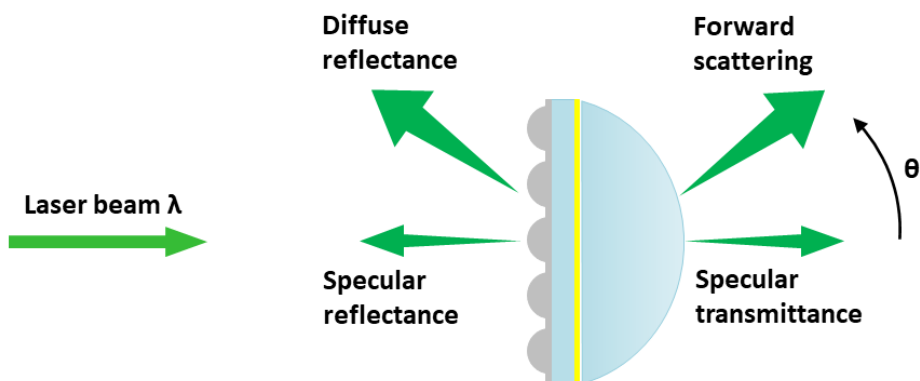
Figure 11. Measurement scheme of angularly resolved scattering.

5.2 Morphology of silica domes and influence of preparation parameters [Papers I, II, III]

One of the aims was to clarify the influence of synthesis parameters on the morphology of structured coating. Depending on the variables, structured silica surfaces with different dome sizes, shapes and surface densities can be prepared.

The analysis presented in the present chapter is based on the observations made in case of spray-coated materials. As described in chapter 4.1, in comparison to spin-coating, spraying adds complexity to the already multi-variable nature of the sol-gel phase separation and involves several additional system parameters. It is also important to point out that the inherent connections between the variables makes it difficult or impossible to isolate the influence of a single parameter. Thus, comparison between the absolute values of dome size characteristics from different series can be misleading and the presented numerical values should be interpreted as manifestation of characteristic trends rather than for deriving universally applicable dependence laws.

Propanol, ethanol and methanol were compared as polar solvents in the sol. Diameter of the obtained domes increased in the same direction as volatility and polarity of the solvent (propanol, ethanol and methanol). Phase separation was found to be poorly controllable in ethanol and methanol systems as spray-coating led to surfaces, where the size, geometry and surface density of formed features varied to a great extent. In some cases, a continuous gel film was formed. This might have been due to a rapid evaporation rate of the solvent which led to faster sol-gel transition compared to the nucleation growth in the sol which was not yet deposited on the substrate. In the case of propanol, principally, the sol-gel transition starts after phase separation onset in the sol layer which is already on the glass substrate. This allows time for silica-rich phase to form droplets before gelling. As uniform coatings were repeatedly produced

only when propanol was used as the solvent, only corresponding samples were included in the analysis of further parameters variation. The main results about the dependence of the surface morphology on system parameters are briefly described in the following sections.

Overall tendencies about correlation of parameters and surface structures are presented in figure 12 and table 1. Influence of amount of sprayed sol (A), alcohol-TEOS volume ratio (T), water-TEOS (R) and catalyst-TEOS (K) molar ratios are going to be discussed. Also, some examples about multilayered structures formed in borderline conditions are shown in figure 12 (m–o).

The amount of solution deposited onto the substrate significantly influenced the dome diameter. Increase of the sprayed sol amount resulted in an increase in the diameter of domes (Fig. 12a–c). It is not directly defined by the sprayed amount, but several other parameters also determine the amount of solution which deposits on the substrate. Solvent viscosity affects the amount of sol that is deposited during a definite time. Latter is also related to concentration of TEOS, water and catalyst in sol. Volatility of a solvent determines to what extent sol evaporates during spraying before depositing onto substrate. Therefore, there are complex dependences between synthesis parameters and results.

Overall tendency with TEOS concentration was that more diluted solutions led to a decrease in the dome diameter. However, the sensitivity towards other parameters also changed with varying concentration. More concentrated (T = 10) solutions were more sensitive to change of water or catalyst amount than solutions with T ≥ 20. When T = 10, the increase in R from 0.5 to 1.5 resulted in more densely positioned domes without notable change in their diameter (Fig. 12g–i). In case of more diluted solutions, there is no change in dome density, but there is an increase in dome diameter from R = 0.5 to R = 1 and no change from R = 1 to R = 2. Increased catalyst concentration in more concentrated sols resulted in the formation of multilayered structures (Fig. 12o). Polycondensation rate within the TEOS-rich domains was high enough to produce gelled silica spheres before settling on the substrate, which enabled the second layer to maintain almost spherical shape. The secondary structures were rather small and flat with more diluted solutions. With T > 20, the diameter of the domes of the bottom layer was found to increase with increasing K (Fig. 12j–l) suggesting that the rate of TEOS polycondensation primarily affects the speed at which nucleated droplets grow and has less significant influence on the number of nucleated TEOS-rich domains.
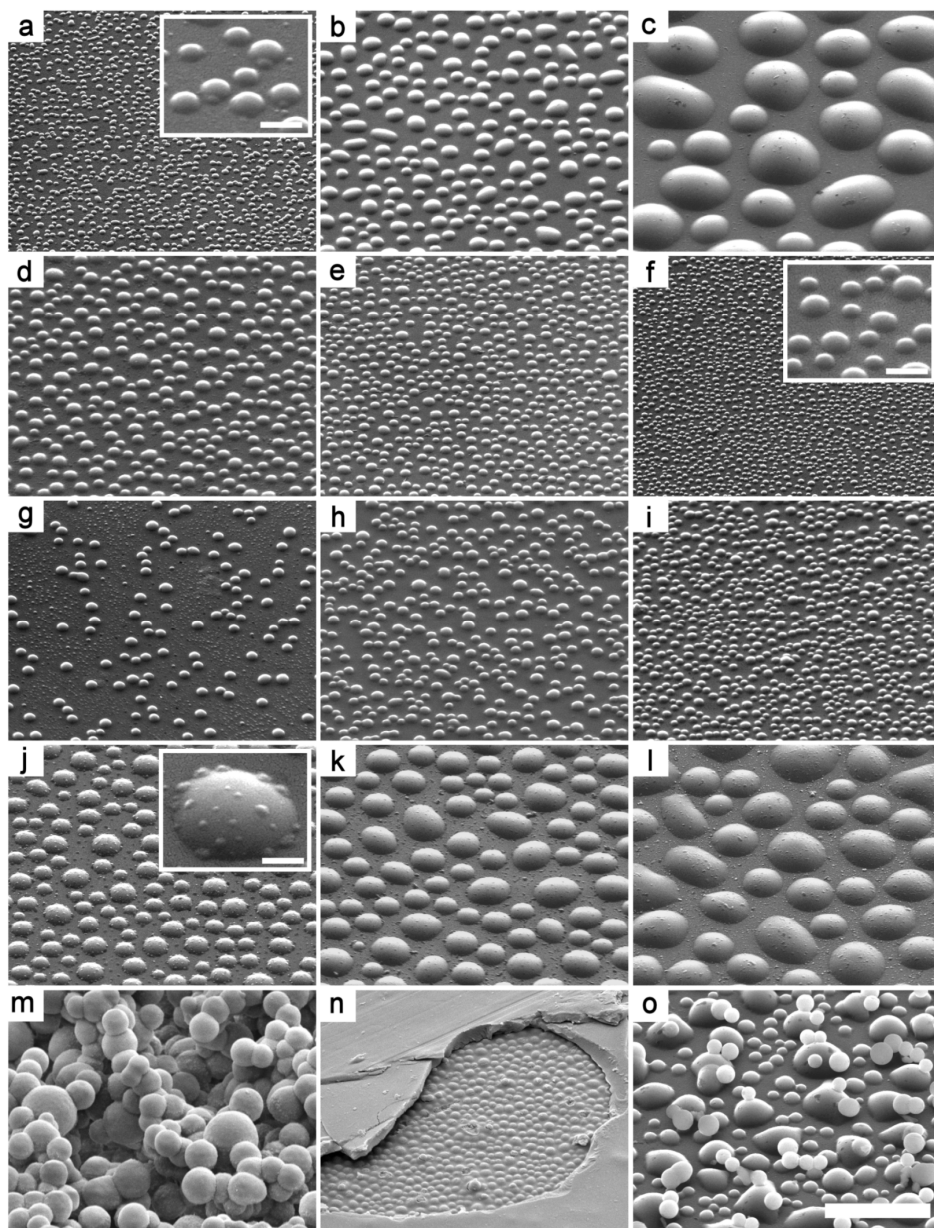
Figure 12. SEM micrographs of representative structured silica surfaces on glass substrate obtained upon the following choice of sol and spray parameters: A=35 μl, 55 μl, 75 μl (a–c); T=10, 15, 20 (d–f); R=0.5, 1, 1.5 (g–i); K=0.05, 0.1, 0.2 (j–l). Silica surfaces formed at borderline conditions: macroporous film with T=1 (m); two-layered structure with R=2 (n); domes with K=0.2 at concentration T=10 (o). The length of the scale bar is 5 μm (for insets 400 nm).

Table 1. The mean roughness of the surfaces of the samples and dimensions and height/width ratios (obtained from AFM and SEM measurements) of the round structural elements on samples obtained using different synthesis parameters.

Variable synthesis parameter	Sample	Other solution parameters	Surface roughness (nm)	Height (nm)	Diameter (nm)	Height/width ratio	No. of domes per 400 μm^2
Amount of sprayed sol	A=35	T=10; R=1; K=0.1	45	74 ± 9	272 ± 44	0.3	1612
	A=55		46	207 ± 25	729 ± 111	0.3	244
	A=75		118	379 ± 80	2866 ± 688	0.1	40
Alcohol-TEOS volume ratio	T=10	R=1; K=0.05	47	164 ± 27	598 ± 126	0.3	416
	T=15		40	144 ± 20	427 ± 77	0.3	504
	T=20		28	88 ± 14	234 ± 37	0.4	1233
Water-TEOS molar ratio	R=0.5	T=10; K=0.05	29	150 ± 25	540 ± 55	0.3	368
	R=1		43	136 ± 26	478 ± 75	0.3	796
	R=1.5		23	75 ± 20	413 ± 57	0.2	1088
HNO$_3$-TEOS molar ratio	K=0.05	T=30; R=1	46	164 ± 24	917 ± 182	0.2	219
	K=0.1		62	203 ± 27	1329 ± 321	0.2	76
	K=0.2		86	281 ± 36	2194 ± 592	0.1	30

Another important sol-gel system parameter is the relative humidity (RH). In series of experiments conducted by spin-coating, relative humidity was varied between 10% and 70%. Overall tendency was that with increasing RH from 10% to 50% the dome density increased. More water molecules from surrounding air lead to faster hydrolysis and condensation reactions of TEOS. Also, solvent evaporation is slower due to higher RH and phase separation can proceed further before gelation. With elevated RH from 50% to 70% the diameter of the domes increased (while dome density decreased), which can be due to slower solvent evaporation and thus, probable joining of smaller droplets.

The relative humidity of the surrounding environment was not purposely controlled during the preparation of coatings. Coating procedures were carried out in an ambient lab environment of 20–49% RH. From application point of view, it might be preferable that the ambient humidity does not have significant influence on material formation as controlling the humidity of the environment would add complicacy and cost to manufacturing. Thus, it would be attractive to develop a synthesis protocol, where the structure forming reactions are controlled and stable in an ambient environment with natural humidity fluctuations.

5.3 Antireflection and light scattering properties of surfaces with silica domes [Paper I]

A set of surfaces with apparently different morphological parameters were chosen from the range of prepared samples for optical characterization. A high packing density and a large height-to-width ratio of domes is expected to yield a more pronounced optical effect [28, 31]. Bearing that in mind six different surfaces presented in figure 13 (samples S1–S6) were selected. These samples were chosen to also present some systematic variations in surface morphology, like having the series of domes with different diameters, change in dome density, and single layer and multistructured surface. It is expected that anti-reflective (AR) or scattering properties occur when the characteristic lengths of the surface features match the Vis-NIR wavelengths of light. The morphological features of samples S1–S6 is presented in table 2.
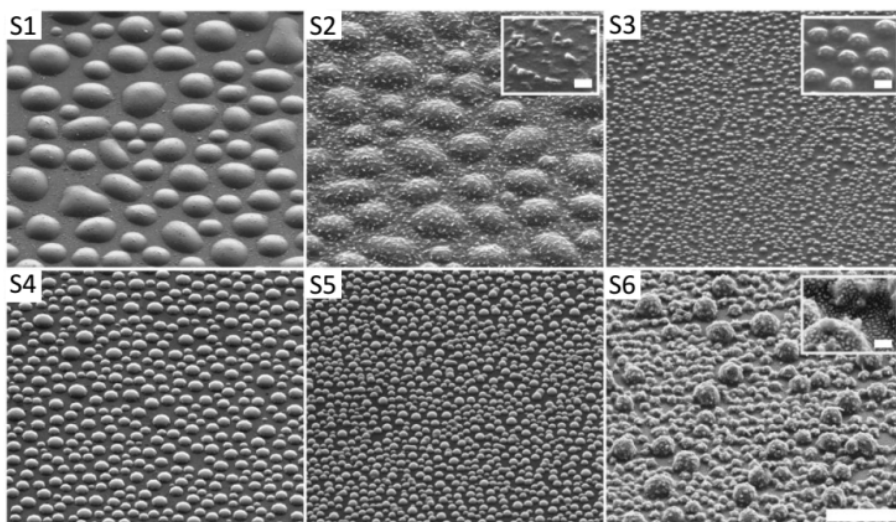
Figure 13. SEM micrographs of structured silica surfaces selected for optical characterization. The length of the scale bar is 5 μm (for inset 300 nm).

Table 2. Morphological characterization (obtained from AFM and SEM measurements) and WCA-s of samples S1–S6. In case of S6 two distinct maxima observed in the size distribution of domes are presented.

Sample	Surface roughness (nm)	Height of domes (nm)	Diameter of domes (nm)	Height/width ratio of domes	No. of domes per 400 μm^2	Water contact angle (°)
S1	86	281 ± 36	2194 ± 592	0.1	30	61
S2	61	189 ± 26	2633 ± 535	0.1	15	57
S3	17	59 ± 11	364 ± 72	0.2	2176	50
S4	67	220 ± 31	829 ±151	0.3	500	66
S5	97	262 ± 39	540 ± 96	0.5	1080	81
S6	168	535 ± 78	666 ± 77 1740 ± 234	0.8	223	132

Diffuse reflectance and scattering properties were measured to explore possible AR and light trapping abilities of the prepared structured surfaces. Vis-NIR diffuse reflectance spectra showed a reduced total reflectance for all structured surfaces compared to a bare glass (Fig. 14). Typical bare glass reflectance (of single surface) is two times lower, as in this type of measurement it was not possible to eliminate the reflectance from the back surface of the glass slide. Thus, the AR effect of the structured coating is probably a lot stronger than

presented in figure 14. But even so, samples S3–S6 had a decrease of reflectance up to 30% compared to the bare glass.

For samples S3–S5 the drop of reflectance clearly peaked at a specific wavelength. In contrast, sample S6 had a quite uniform AR effect over the whole Vis-NIR spectral range. This is explained by a relatively narrow size distribution of the domes in samples S3–S5 whereas sample S6 had the multi-scale hierarchical roughness of domes, which enables AR effect over a wider range of wavelengths. Relatively good performance of sample S5 may be due to a more dense packing of the domes. Samples S1 and S2 had the wide flat domes and they had least effect on the lowering the reflectance. Even though sample S2 had an additional surface roughness, it only slightly improved the AR.
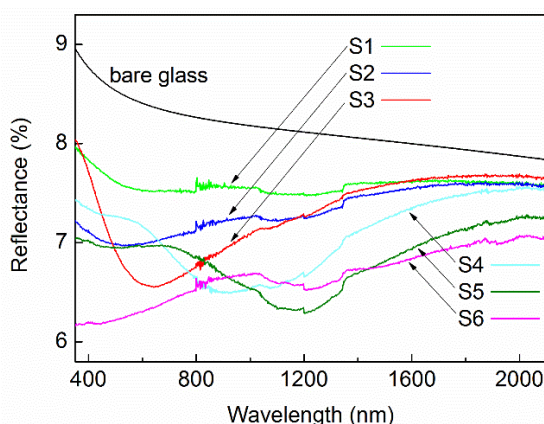
Figure 14. Diffuse reflectance spectra of glass slides covered with the silica structures.

To study the possible light trapping capabilities of the structured coatings, the forward scattering was explicitly studied for samples S2, S3, S4 and S6, which had the reflectance minima in or close to the visible spectral range (Fig. 15). An incident laser wavelength close to the reflectance minimum was selected. Sample S6 had the best forward scattering performance. In this case most of the incident light was scattered in the angular range 5–25° and specular transmittance was relatively small. In accordance to these properties, the sample did not transfer optical image. Multi-scale roughness occurred also in the case of sample S2, similarly to S6, but the domes of the first layer were too flat whereas the domes of the second layer were situated too sparsely. Therefore, the specular transmittance was notably more intense compared to the scattered light. Sample S3, and to some extent also S4, had the least effective scattering (even though their antireflective properties were comparatively good). The silica structures on those surfaces (particularly S3) are sufficiently small, uniform and close packed so that the surface looks optically homogeneous and does not affect specular transmittance noticeably. The results are in accordance with the observable translucency of the slides.
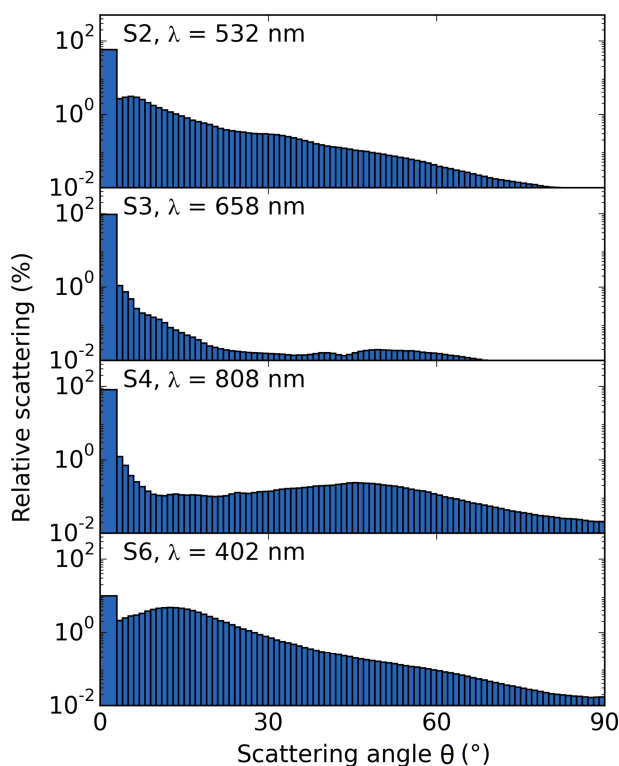
Figure 15. Angular dependence of the forward scattered light (relative intensity per solid angle spanned by 1° of linear angular range). Laser beam of the indicated wavelength was perpendicularly incident on the structured surface.

5.4 Wetting properties of surfaces with silica domes [Paper I]

Water contact angles (WCA) seen in figure 16 were evaluated from the same surfaces, which were optically characterized, namely S1–S6 (Fig. 13 and table 2). S1 (61°) and S2 (57°) had similar WCA-s while having dome diameters in the same size range, whereby the double structures of S2 did not improve the WCA probably due to their low packing density. The smallest domes in S3 resulted in lowest WCA 50°, which had also rather small height to width ratio. S5 with WCA 81° had slightly larger height-width ratio and packing density of domes compared to S1–S4. S6 had significantly larger WCA 132° as S1–S5 had quite similar WCA-s 50°–80°. It seems that the greater height-to-width ratio and presence of multi-scale roughness of the domes improve the hydrophobic behavior notably. S6 had both properties leading to a better hydrophobicity compared to the other samples.
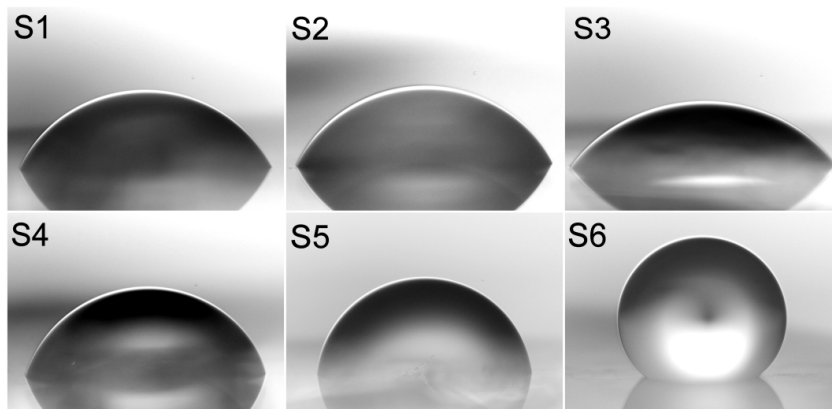
Figure 16. Photographs of water droplets on samples S1–S6 (for morphology see figure 13).

It is necessary to point out that the surface energy of silica is quite high, which means that silica surface is inherently hydrophilic. To demonstrate that, smooth film was prepared from aged TEOS solution, where no phase separation occurred, and this reference coating had WCA 25° [95]. This supports the conclusion that the altered wetting behavior of the structured surfaces is the effect of surface morphology only. Accordingly, additional covering of S6 with low surface energy coating (e.g. fluoropolymer) would most likely lead to a superhydrophobic surface (WCA > 150°).

5.5 Silica structured surfaces as cell growth substrates [Paper III]

Topographic interactions between normal primary cells – fibroblasts extracted from human skin and round silica structures were studied to evaluate the biocompatibility of the coatings. More precisely, the spreading and growth of cultivated primary cells were studied on patterned substrates with different nano- and microstructures. Fluorescence microscopy and SEM analysis were applied to evaluate cell viability, adhesion, migration and spreading on prepared surfaces. The morphology of the samples selected for cell experiments are shown in figure 17 whereas the characteristics of different surface structures are described in table 3. Different silica patterns were in this case obtained by changing the solvent and TEOS concentration in the precursor solution. Smooth sol-gel silica coating and bare borosilicate glass (commonly used for cell culturing) substrates were used as a reference in cell experiments.
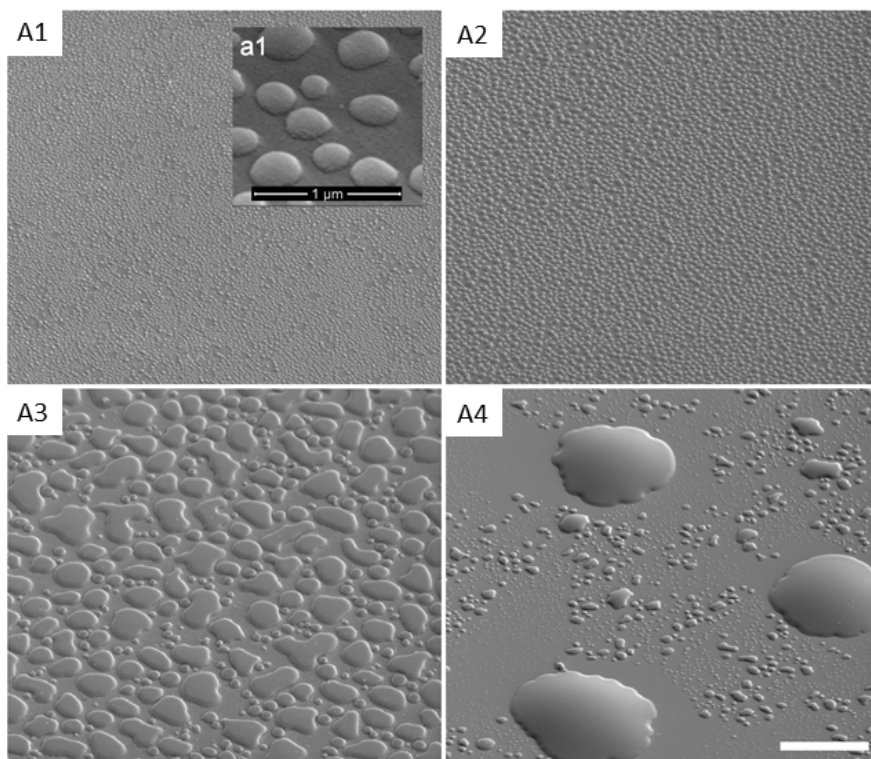
Figure 17. SEM micrographs of silica domes in different sizes for cell experiments. The length of the scale bar is 10 µm. The inset a1 shows a magnified area of A1 surface.

Table 3. The characteristics of silica structures selected for cell experiments (obtained from AFM and SEM measurements).

Sample	Mean diameter of domes (µm)	Mean height of domes (nm)	No. of domes per 10 000 µm^2	Water contact angle (°)
A1	0.2	90	51 000	48
A2	0.5	210	24 000	54
A3	1	200	4300	15
A4	10	920	18	34

In figure 18, fluorescence microscopy images are presented to demonstrate the fibroblasts growth on different patterned surfaces (Fig. 18a–d) and on references (Fig. 18e, f). The cell viability was evaluated through characterization of cell shape, whether it is normal or atypical: enlarged, spindle shaped or narrowed (Fig. 18g–i). On a flat surface, fibroblasts usually maintain their "normal" spindle-shaped morphology (Fig. 18h). The proportion of abnormal cells grown on A1 and A2 was similar to the amount of atypical cells on the flat surfaces (Fig. 19a).

In contrast, cells grown on A3 and A4 displayed increased proportion of enlarged cells and decreased proportion of cells with narrow cytoplasm. Typically such cells do not proliferate and represent probably either senescent (enlarged cells) or stressed cells (narrow cytoplasm) [96]. The reason why fibroblasts grown on A3 and A4 surfaces contained more enlarged and senescent cells (Fig. 19b) is likely related to either attachment deficit or disturbance of normal cytoskeleton (Fig. 18c, d). Cytoskeleton disturbance by domes is clearly seen in case of A4 from fluorescence microscopy image (Fig. 18d, red arrows mark the domes), and less in case of A3 (Fig. 18c). Attachment deficit of A3 has been revealed when studying cross-sections of fibroblasts growing on domes.
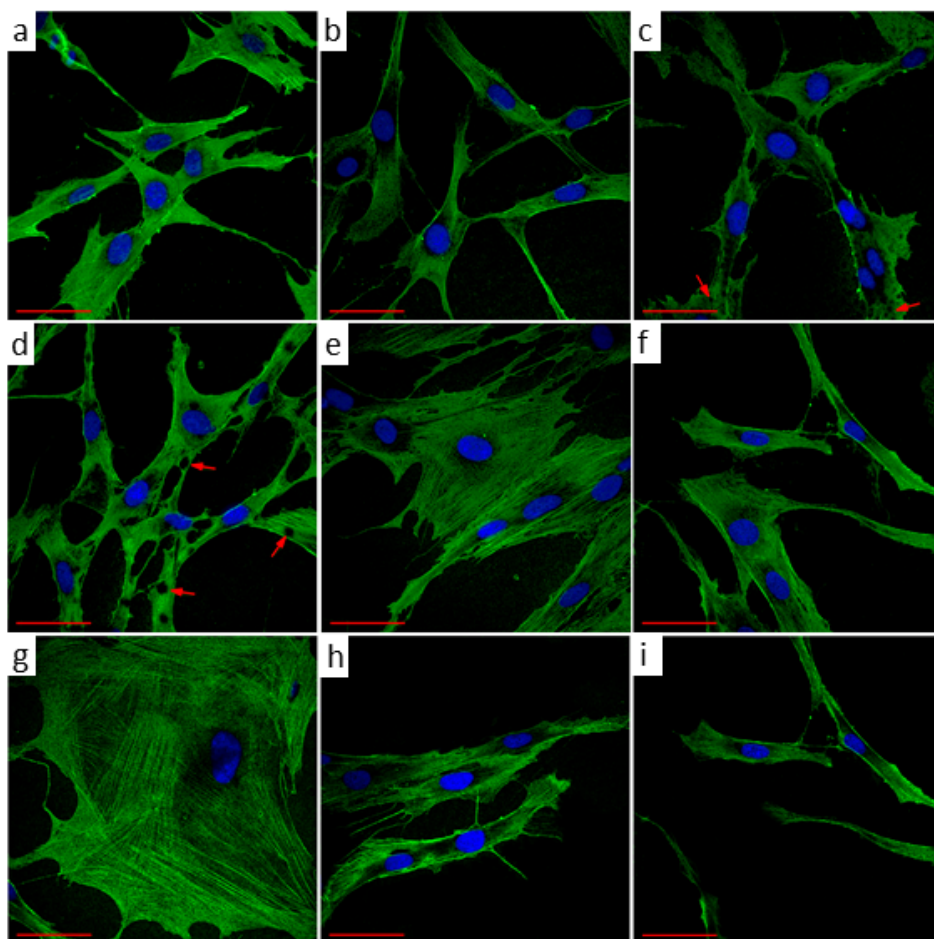
Figure 18. Confocal fluorescence microscopy images of fibroblasts cultured on silica domes A1–A4 (a–d), smooth silica surface (e) and glass (f), with visible gamma-actin (green) and nuclei (blue). Red arrows mark location of domes. Confocal fluorescence images of fibroblasts with different morphology: g – enlarged cell; h – spindle shape (normal) cells; i – narrow cells. The length of the scale bars is 50 µm.
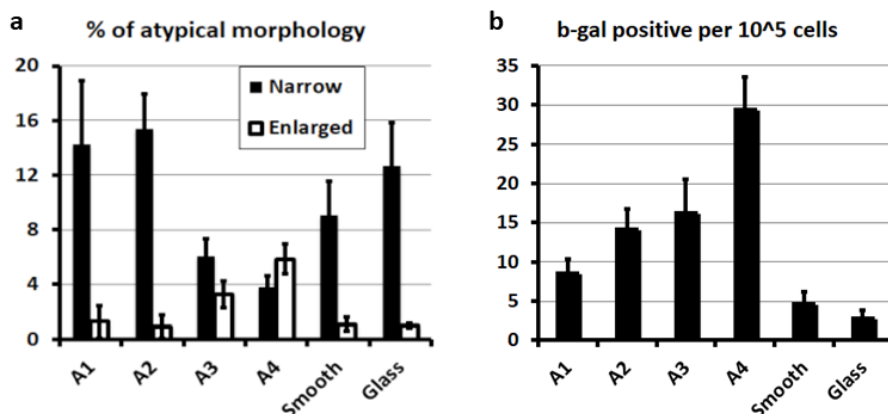
Figure 19. Graphs describe the percentage of cells with atypical morphology (a) and ratio of SA-b-gal positive per 10^5 normal cells, which indicate existence of senescent cells (b). Error bars ± SD.

Attachment of cells to the substrate was studied by cutting fibroblasts on silica domes with FIB-SEM. Vertical cuts of the cell-substrate interfaces are seen in figure 20. Cells grown on A1 and A4 displayed tight attachment to the substrate. On A1 the domes were small enough that they were integrated into the cell membrane. But in the case of A4, comparatively wide and flat domes had wide bending angle which allowed cells easily to spread over the domes. On A2 and A3 the fibroblasts attached only to the top of domes which can be due to inability of the cell's cytoskeleton to bend between these domes. There-fore, the contact surface is decreased between fibroblast and the patterned surface and this can result in a decrease in the number of anchoring points. However, on A2 there is tendency that there are slightly less senescent cells than on A3 (Fig. 19b), maybe because more closely situated domes of A2 enable to form more anchoring points between cells and domes.

Spreading and growth characteristics of fibroblasts indicated biocompatibi-lity of the prepared coatings. It is important to point out that the observed changes in cell morphology were due to different surface roughness only as the surface chemistry is the same all over the different substrates (on the domes and the areas between them). The increase in the size of the structural elements presented to the cells in this work thus led to increased inhibition of cell growth, altered morphology and enhancement of cell senescence.
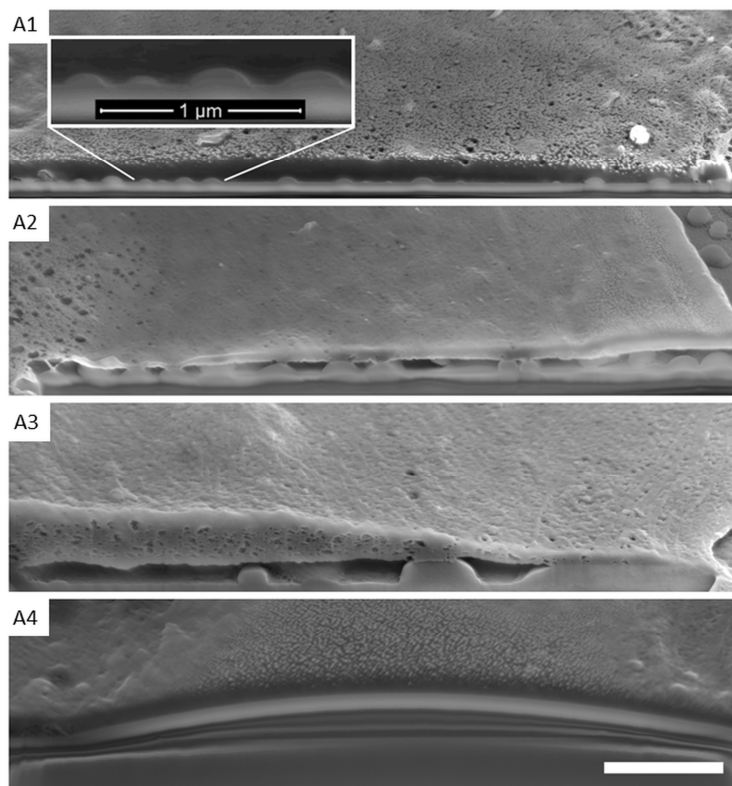
Figure 20. SEM micrographs of cross-sections of fibroblasts on different silica domes. This figure indicates cell-surface integration between different sizes of domes. The length of the scale bar is 2 μm.

5.6 Morphology of silica foam and influence of preparation parameters [Paper IV]

The influence of different parameters on foam formation were studied to find the preparation conditions for high quality foams. The foam should be homogenous, have no cracks and have as small bulk density as possible. Visual inspection, optical microscopy and SEM were used to evaluate the quality.

H_2O_2 concentration was varied from 10 to 70 wt.% in sol. The highest quality foams were prepared by using 30% or 40% of H_2O_2 and hereafter 30% H_2O_2 was used for investigating the influence of different parameters on foam formation. By using different alcohols as solvents, methanol, ethanol, 1-propanol, 1-butanol and 1-pentanol (Fig. 21a–e), foams obtained by using propanol exhibited the most uniform morphology. Other alcohols used as a solvent caused problems with foam quality. 1-butanol and 1-pentanol resulted in cracked samples during aging and drying and although all films exhibited a pore diameter gradient along the thickness of the foam, the effect was more evident

with ethanol and methanol. Therefore 1-propanol was used to study the solvent concentration influence on the properties of the films and to vary film thickness.

Solvent concentration in the sol did not correlate well with the film thicknesses. Variation with 1-propanol/TMOS molar ratios of 0.1, 0.3, 0.5 and 0.7 resulted in film thicknesses of 273, 309, 239 and 171 µm, correspondingly. Also, different bulk densities of foams were obtained and the smallest measured bulk density was 68.3 kg/m^3 with solvent/TMOS molar ratio 0.5. Higher solvent concentration resulted in too light foam and it was not possible to measure the mass accurately for calculating bulk density. At lower solvent concentrations the pore diameter gradient occurred similarly to the use of methanol.

Film thicknesses were also studied by varying the amount of sprayed solution from 100 µl to 550 µl (Fig. 21f, g). The optimum for a good foam sample was 400–500 µl, as smaller amount did not result in proper foam forming or resulted in cracked film, and more than 500 µl resulted in foam destruction by prolonged aerosol deposition.
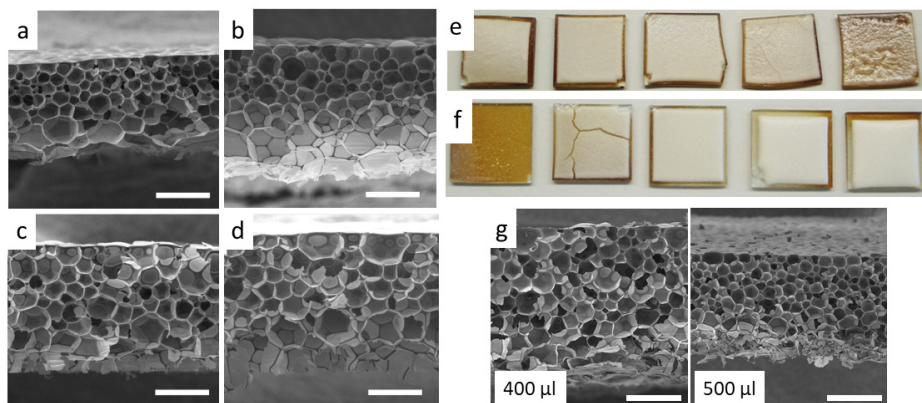
Figure 21. SEM micrographs of cross-sections of foam films prepared with different solvents: a) methanol; b) ethanol; c) 1-propanol; d) 1-butanol. The scale bar for a)–d) is 100 µm. e) Photograph of foams prepared by using (from left to right) methanol, ethanol, 1-propanol, 1-butanol or 1-pentanol as a solvent. f) Photograph of silica foams prepared by using (from left to right) 100, 200, 300, 400 or 500 µl of sol for film preparation. g) SEM micrographs of cross-sections of foam films prepared using 400 or 500 µl of sol. The length of the scale bar is 200 µm.

As previously mentioned the cross-sections of the foams were not homogeneous. There was a diameter gradient of the pores so that the bigger bubbles were near the substrate and the smaller ones near the surface. This size difference is caused by faster sol gelation near the surface due to evaporation-induced solvent concentration decrease and exposure to ambient humidity. Also the bubble coarsening is reduced as less gas is able to reach to the upper layer of film.

These silica foams have a closed-cell macroporous structure with bulk density similar to aerogels. This morphology can be superior for thermal insulation properties as materials with closed-cell porosity have very low thermal conductivities. Furthermore, the silica foam preparation only includes spray-coating of sol onto catalyst-coated substrate and annealing. Traditional aerogel formation with solvent exchange and supercritical drying of wet gels can be a lot more time-consuming and expensive process.

5.7 Thermal conductivity of silica foam [Paper IV]

Foams with different thicknesses were prepared for thermal conductivity measurements (table 4). The sprayed sol was synthesized with 1-propanol/ TMOS molar ratio 0.3 and 30 wt.% H_2O_2 aqueous solution. The amount of sol was varied to obtain different thicknesses. Corresponding SEM images of the foam films used for thermal conductivity measurements are presented on figure 22. The lowest measured thermal conductivity of the prepared foams was 0.018 ± 0.001 W/(m·K), which is also similar to silica aerogels. These measurements demonstrate that the prepared silica foam materials are potentially applicable as efficient thermal insulation materials.

Table 4. Thermal conductivity of foams with different parameters.

Sample	Sol amount (μl)	Foam thickness (μm)	Bulk density (kg/m^3)	Thermal conductivity (W/(m·K))
A	300	304	87.5	0.022
B	400	393	91.4	0.021
C	450	339	143	0.018
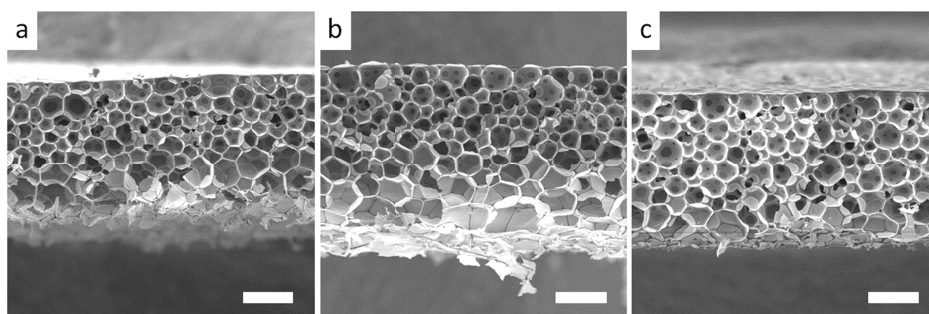
Figure 22. SEM images of the cross-sections of the silica foam films used for thermal conductivity measurements. The films were prepared by using 300 μl (a), 400 μl (b), and 450 μl (c) of sol. Scale bars correspond to 100 μm.

6 PROSPECTS AND CHALLENGES

Results of the present thesis show the potential of the applied sol-gel phase separation method as a single-step coating technology, which enables to prepare multifunctional structured coatings with simultaneous optical and superhydrophobic functionality. In addition, as demonstrated, spray-coating can be used to coat large areas, allowing more straightforward scale-up than conventional lithography methods that have been applied in scientific studies where similar surface features are prepared. Although the development of industrial spraying was beyond the scope of present work, we tested an industrial spray coater (sample S6, Fig. 13). As seen on the SEM micrograph, surface features with a large height to width ratio were formed, and they could provide superior optical and wetting properties. Considering the simplicity and scalability of the material preparation, these coatings could be attractive for window glass, for example. However, presented preliminary results show that spraying leads to results that are significantly different from spin-coated samples, especially in the case of industrial spray coater. Thus, while it is possible to draw conclusions about the nature and general controllability of the processes, different application methods and devices need separate thorough optimization of process parameters.

When speaking of improving optical and wetting properties of the structured surface, there are some limitations. Surfaces with peak-like structures show a lot better performance according to literature [97]. Due to the nature of the present technique the height of the surface structures cannot exceed the diameter because of the spherical shape of the initial droplet. However, as seen in several experiments, even a single-cycle coating can have multi-scale structuring. This possibility needs further studies in follow-up studies as significant advancement in the hydrophobicity of the coatings could be possible achieved by closer mimicry of superhydrophobic Lotus structure, especially in combination with subsequent surface energy-lowering treatments.

Although fibroblasts grew on all studied surfaces we decided to continue our following studies with more elastic materials because fibroblasts' natural environment is soft tissue [98]. There might be better results when silica-based materials used as substrates for cells originate from hard tissues such as bone, because Young's modulus of bone tissue is in the same magnitude as silica.

Bulk densities and thermal conductivities of the prepared foams are comparable to silica aerogels. However, from application point of view the film thickness presents limitation. In our experiments the maximum film thickness is limited to ~550 μm, because due to elongated spraying times in the case of larger required sol quantities, the depositing aerosol started to destroy the forming foam.

7 CONCLUSIONS

In the present thesis two differently microstructured silica coatings were introduced, where the material formation is based on concurrent phase separation and sol–gel transition processes. The main focus was on the structured silica coating with a layer of round micro- and nanodomes, whereas the topic of macroporous silica foam film was covered more briefly. In both preparation processes, the increase in precursor solution viscosity is the key to the microstructure formation and the final morphology is determined by the freezing of structure evolution due to sol-gel transition. In the case of surface coating with domes, the structuring was formed through a continuous separation of the silica-rich phase from the sol. The foam film coating was prepared with the help of purposely created gas phase into the sol.

Sol-gel phase separation method together with spray-coating is a promising bottom-up technique for preparing structured functional silica surfaces and is potentially suitable for covering large surfaces. It was demonstrated that by choosing suitable alkoxide concentration, solvent type, water- and catalyst-alkoxide molar ratios and also relative humidity, it is possible to vary the size, shape and surface density of the domes. Uniform coatings were repeatedly produced only when 1-propanol was used as the solvent. However, the controllability of developed methods remains a challenge due to the self-progressing and stochastic nature of underlying chemical and physical processes. Nevertheless, depending on the preparation conditions, it is possible to obtain surface patterning which has a resemblance to the moth-eye structures. Sufficiently dense packing of silica domes in sub-μm range and multilayered coating led to notable antireflection and light scattering effects in the Vis-NIR spectral range. Decrease of reflectance up to 30% compared to the bare glass was achieved. As some of the produced silica surfaces had water contact angles exceeding 130°, simultaneous superhydrophobicity (contact angle > 150°) can be achieved by further surface functionalization (e.g. with fluoropolymer). The surfaces were also found to be biocompatible and it was shown that growth characteristics and morphology of fibroblasts is influenced by the morphology of the substrate.

Sol-gel process together with catalytic decomposition of hydrogen peroxide is a novel method for the preparation of thick silica foam film, where well-defined closed-cell porosity appears. The smallest measured bulk density was 68.3 kg/m^3 and the lowest measured thermal conductivity was 0.018 W/(m·K). Macroporous characteristics of the prepared foam are similar to silica aerogels and therefore, it is a good candidate for high-temperature thermal insulating material.

SUMMARY IN ESTONIAN

Mikrostruktuursete ränioksiidsete sool-geel materjalide arendamine ja funktsionaalsete omaduste hindamine

Käesolevas doktoritöös kirjeldame kahe mikrostruktuurse ränioksiidse materjali valmistamist, seaduspärasusi selle käigus toimuvates protsessides ja hindame saadud materjalide olulisi funktsionaalseid omadusi erinevates potentsiaalsetes rakendustes. Nimetatud materjalide mikrostruktuur tekib samaaegselt kulgevate ränialkoksiidse lähteaine faasilise koostise evolutsiooni ja soolist geeliks muundumise koosmõjul. Töö põhirõhk on ränioksiidsetel ümarate mikro- ja nanostruktuuridega pinnetel ning lisaks käsitletakse ränioksiidset makropoorset vahtu. Mõlema materjali struktuur hakkab tekkima tänu lähtelahuse viskoossuse suurenemisele ja lõpliku struktuuri määrab sool-geel ülemineku hetk. Ümarad pinnastruktuurid tekivad ränioksiidi moodustava faasi eraldumisel soolist, vahukile saadakse sooli sisse gaasilise faasi tekitamise teel.

Töös tutvustatav sool-geel-faasieralduse meetod on perspektiivikas alt-ülesmeetod, millega saab valmistada funktsionaalseid struktuurseid ränioksiidseid pindeid ning pihustamine võimaldab selle meetodi kasutamist suurte pindade katmiseks tööstuslikus skaalas. Doktoritöös näitasime, et ümaraid pinnastruktuure saab valmistada erineva suuruse, kuju ja pindtihedusega, ja uurisime tekkiva pinde morfoloogia varieerumist sõltuvalt alkoksiidi kontsentratsioonist, lahustist, vee ja alkoksiidi moolsuhtest, katalüsaatori ja alkoksiidi moolsuhtest ning suhtelisest õhuniiskusest. Korratavalt saadi kõige ühtlasemad pinded lahustina 1-propanooli kasutades. Struktuursete pindade võimalikku optilist funktsionaalsust silmas pidades valmistati pinded, mis on sarnased looduses leiduvate optiliste struktuuridega (nt. koiliblika silm). Erinevas suurusjärgus struktuursusega pinded, mille elementide diameeter on alla mikromeetri ja pindtihedus võrdlemisi suur, omasid märkimisväärseid peegeldumisvastaseid ja valguse hajumist muutvaid omadusi nähtavas ja lähi-infrapunases spektrialas. Näiteks vähenes tagasipeegeldumine struktuurselt pinnalt 30% võrreldes katmata klaasiga. Samuti hinnati valmistatud pinnete märgumisomadusi. Vee kontaktnurk ületas mõnede proovide puhul 130°, seega on ilmselt võimalik pinna täiendava keemilise modifitseerimisega (nt. fluoropolümeeriga katmise teel) saavutada superhüdrofoobsus (kontaktnurk üle 150°). Lisaks näidati doktoritöös, et valmistatud mikro- ja nanostruktuursed pinnad on biosobivad ning nende struktuursus omab bioaktiivset mõju, kuna rakkude kasv ja paljunemine sõltuvad substraadi struktuuride läbimõõdust ja pindtihedusest.

Ränialkoksiidsüsteemis toimuvaid keemilisi ja füüsikalisi protsesse kasutati ka kombinatsioonis katalüütilise vesinikperoksiidi lagunemisega, et valmistada ränioksiidseid makropoorseid vahte, millel on hästi defineeritud suletud poorsus. Saadud vahtude makropoorne struktuur on sarnane aerogeelidega. Vähim saavutatud massitihedus oli 68.3 kg/m^3 ja soojusjuhtivus 0.018 W/(m·K). Selliste omadustega materjal võib leida kasutust kõrgetemperatuurilise soojusisolatsioonimaterjalina.

REFERENCES

[1] K. Saal, T. Tätte, M. Järvekülg, V. Reedo, A. Lõhmus, I. Kink, Micro- and nano-scale structures by sol-gel processing, *International Journal of Materials & Product Technology* 40 (2011) 2–14.

[2] V. Kiisk, T. Kangur, M. Paalo, T. Tätte, S. Lange, S. Pikker, I. Sildos, Structural and luminescence characteristics of SnO_2:Eu and SnO_2:Eu,Sb nanophosphors upon annealing at high temperatures, *Materials Chemistry and Physics* 130 (2011) 293–298.

[3] V. Kisand, J. Shulga, T. Tätte, U. Visk, M. Natali, G. Mistura, M. Paalo, M. Lobjakas, I. Kink, Preparation of structured sol-gel films using tape casting method, *Materials Science and Engineering B – Solid State Materials for Advanced Technology* 137 (2007) 162–165.

[4] A. S. Dorcheh, M. H. Abbasi, Silica aerogel; synthesis, properties and characterization, *Journal of Materials Processing Technology* 199 (2008) 10–26.

[5] S. Dire, V. Tagliazucca, E. Callone, A. Quaranta, Effect of functional groups on condensation and properties of sol-gel silica nanoparticles prepared by direct synthesis from organoalkoxysilanes, *Materials Chemistry and Physics* 126 (2011) 909–917.

[6] P. C. A. Jeronimo, A. N. Araujo, M. C. B. S. M. Montenegro, Optical sensors and biosensors based on sol-gel films, *Talanta* 72 (2007) 13–27.

[7] K. Sumida, K. Liang, J. Reboul, I. A. Ibarra, S. Furukawa, P. Falcaro, Sol-Gel Processing of Metal-Organic Frameworks, *Chemistry of Materials* 29 (2017) 2626–2645.

[8] D. Wang, G. R. Bierwagen, Sol-gel coatings on metals for corrosion protection, *Progress in Organic Coatings* 64 (2009) 327–338.

[9] A. L. Penard, T. Gacoin, J. P. Boilot, Functionalized sol-gel coatings for optical applications, *Accounts of Chemical Research* 40 (2007) 895–902.

[10] D. Arcos, M. Vallet-Regi, Sol-gel silica-based biomaterials and bone tissue regeneration, *Acta Biomaterialia* 6 (2010) 2874–2888.

[11] T. Tätte, T. Avarmaa, R. Lõhmus, U. Mäeorg, M. E. Pistol, R. Raid, I. Sildos, A. Lõhmus, Transparent and conductive Sb-doped tin oxide SPM tips prepared by sol-gel method, *Materials Science & Engineering C* 19 (2002) 101–104.

[12] V. Kiisk, I. Sildos, S. Lange, V. Reedo, T. Tätte, M. Kirm, J. Aarik, Photoluminescence characterization of pure and Sm^{3+}-doped thin metaloxide films, *Applied Surface Science* 247 (2005) 412–417.

[13] M. Eltermann, K. Utt, S. Lange, R. Jaaniso, Sm^{3+} doped TiO2 as optical oxygen sensor material, *Optical Materials* 51 (2016) 24–30.

[14] L. Puust, V. Kiisk, M. Eltermann, H. Mändar, R. Saar, S. Lange, I. Sildos, L. Dolgov, L. Matisen, R. Jaaniso, Effect of ambient oxygen on the photoluminescence of sol-gel-derived nanocrystalline ZrO_2:Eu,Nb, *Journal of Physics D-Applied Physics* 50 (2017) 215303.

[15] M. Järvekülg, R. Välbe, J. Jõgi, A. Salundi, T. Kangur, V. Reedo, J. Kalda, U. Mäeorg, A. Lõhmus, A. E. Romanov, A sol-gel approach to self-formation of microtubular structures from metal alkoxide gel films, *Physica Status Solidi A – Applications and Materials Science* 209 (2012) 2481–2486.

[16] M. Part, K. Hanschmidt, J. Jõgi, E. Rauwel, G. A. Seisenbaeva, V. G. Kessler, T. Tätte, Study of the curing mechanism of metal alkoxide liquid threads for the

synthesis of metal oxide fibers or microtubes, *Rsc Advances* 4 (2014) 12545–12554.

[17] B. Polyakov, M. Antsov, S. Vlassov, L. M. Dorogin, M. Vahtrus, R. Zabels, S. Lange, R. Lohmus, Mechanical properties of sol-gel derived SiO_2 nanotubes, *Beilstein Journal of Nanotechnology* 5 (2014) 1808–1814.

[18] M. Timusk, M. Järvekülg, A. Salundi, R. Lõhmus, S. Leinberg, I. Kink, K. Saal, Optical properties of high-performance liquid crystal-xerogel microcomposite electro-optical film, *Journal of Materials Research* 27 (2012) 1257–1264.

[19] B. J. J. Zelinski, D. R. Uhlmann, Gel technology in ceramics, *Journal of Physics and Chemistry of Solids* 45 (1984) 1069–1090.

[20] L. L. Hench, J. K. West, THE SOL-GEL PROCESS, *Chemical Reviews* 90 (1990) 33–72.

[21] A. E. Danks, S. R. Hall, Z. Schnepp, The evolution of 'sol-gel' chemistry as a technique for materials synthesis, *Materials Horizons* 3 (2016) 91–112.

[22] K. Nakanishi, Pore Structure Control of Silica Gels Based on Phase Separation, *Journal of Porous Materials* 4 (1997) 67–112.

[23] K. Kajihara, S. Kuwatani, R. Maehana, K. Kanamura, Macroscopic Phase Separation in a Tetraethoxysilane-Water Binary Sol-Gel System, *Bulletin of the Chemical Society of Japan* 82 (2009) 1470–1476.

[24] K. Nakanishi, N. Soga, Phase Separation in Gelling Silica Organic Polymer Solution: Systems Containing Poly(sodium styrenesulfonate), *Journal of the American Ceramic Society* 74 (1991) 2518–2530.

[25] K. Nakanishi, N. Tanaka, Sol-gel with phase separation. Hierarchically porous materials optimized for high-performance liquid chromatography separations, *Accounts of Chemical Research* 40 (2007) 863–873.

[26] K. Nakanishi, Sol-gel process of oxides accompanied by phase separation, *Bulletin of the Chemical Society of Japan* 79 (2006) 673–691.

[27] C. Triantafillidis, M. S. Elsaesser, N. Husing, Chemical phase separation strategies towards silica monoliths with hierarchical porosity, *Chemical Society Reviews* 42 (2013) 3833–3846.

[28] Y. Chen, M. Elshobaki, R. Gebhardt, S. Bergeson, M. Noack, J.-M. Park, A. C. Hillier, K.-M. Ho, R. Biswas, S. Chaudhary, Reducing optical losses in organic solar cells using microlens arrays: theoretical and experimental investigation of microlens dimensions, *Physical Chemistry Chemical Physics* 17 (2015) 3723–3730.

[29] F. L. Gonzalez, M. J. Gordon, Enhancing near-infrared light absorption in PtSi thin films for Schottky barrier IR detectors using moth-eye surface structures, *Optics Letters* 40 (2015) 1512–1515.

[30] X. Zhao, Y. Sun, J. Bu, S. Zhu, X. C. Yuan, Microlens-array-enabled on-chip optical trapping and sorting, *Applied Optics* 50 (2011) 318–322.

[31] A. Ingenito, O. Isabella, M. Zeman, Nano-cones on micro-pyramids: modulated surface textures for maximal spectral response and high-efficiency solar cells, *Progress in Photovoltaics* 23 (2015) 1649–1659.

[32] S. K. Srivastava, P. Singh, M. Yameen, P. Prathap, C. M. S. Rauthan, Vandana, P. K. Singh, Antireflective ultra-fast nano scale texturing for efficient multicrystalline silicon solar cells, *Solar Energy* 115 (2015) 656–666.

[33] S. Ji, K. Song, N. Thanh Binh, N. Kim, H. Lim, Optimal Moth Eye Nanostructure Array on Transparent Glass Towards Broadband Antireflection, *Acs Applied Materials & Interfaces* 5 (2013) 10731–10737.

[34] J. D. Myers, W. Cao, V. Cassidy, S.-H. Eom, R. Zhou, L. Yang, W. You, J. Xue, A universal optical approach to enhancing efficiency of organic-based photo-voltaic devices, *Energy & Environmental Science* 5 (2012) 6900–6904.

[35] R. Dewan, S. Fischer, V. B. Meyer-Rochow, Y. Oezdemir, S. Hamraz, D. Knipp, Studying nanostructured nipple arrays of moth eye facets helps to design better thin film solar cells, *Bioinspiration & Biomimetics* 7 (2012).

[36] V. E. Ferry, M. A. Verschuuren, M. C. van Lare, R. E. I. Schropp, H. A. Atwater, A. Polman, Optimized Spatial Correlations for Broadband Light Trapping Nano-patterns in High Efficiency Ultrathin Film a-Si:H Solar Cells, *Nano Letters* 11 (2011) 4239–4245.

[37] A. Chandra, G. Anderson, S. Melkote, W. Gao, H. Haitjema, K. Wegener, Role of surfaces and interfaces in solar cell manufacturing, *Cirp Annals – Manufacturing Technology* 63 (2014) 797–819.

[38] K. Yu, T. Fan, S. Lou, D. Zhang, Biomimetic optical materials: Integration of nature's design for manipulation of light, *Progress in Materials Science* 58 (2013) 825–873.

[39] C.-H. Sun, P. Jiang, B. Jiang, Broadband moth-eye antireflection coatings on silicon, *Applied Physics Letters* 92 (2008).

[40] S. J. Wilson, M. C. Hutley, The Optical Properties of Moth-Eye antireflecion Surfaces, *Optica Acta* 29 (1982) 993–1009.

[41] J. Hiller, J. D. Mendelsohn, M. F. Rubner, Reversibly erasable nanoporous anti-reflection coatings from polyelectrolyte multilayers, *Nature Materials* 1 (2002) 59–63.

[42] W. H. Koo, S. M. Jeong, F. Araoka, K. Ishikawa, S. Nishimura, T. Toyooka, H. Takezoe, Light extraction from organic light-emitting diodes enhanced by sponta-neously formed buckles, *Nature Photonics* 4 (2010) 222–226.

[43] J. Bingi, V. M. Murukeshan, Plasmonic nanopillar coupled two-dimensional ran-dom medium for broadband light trapping and harvesting, *Journal of Nanophoto-nics* 9 (2015).

[44] D. G. Stavenga, S. Foletti, G. Palasantzas, K. Arikawa, Light on the moth-eye corneal nipple array of butterflies, *Proceedings of the Royal Society B – Biological Sciences* 273 (2006) 661–667.

[45] M. Manca, A. Cannavale, L. De Marco, A. S. Arico, R. Cingolani, G. Gigli, Durable Superhydrophobic and Antireflective Surfaces by Trimethylsilanized Silica Nanoparticles-Based Sol-Gel Processing, *Langmuir* 25 (2009) 6357–6362.

[46] Y. Xiu, F. Xiao, D. W. Hess, C. P. Wong, Superhydrophobic optically transparent silica films formed with a eutectic liquid, *Thin Solid Films* 517 (2009) 1610–1615.

[47] S. Das, C. Banerjee, A. Kundu, P. Dey, H. Saha, S. K. Datta, Silica nanoparticles on front glass for efficiency enhancement in superstrate-type amorphous silicon solar cells, *Journal of Physics D – Applied Physics* 46 (2013).

[48] J. van de Groep, P. Spinelli, A. Polman, Single-Step Soft-Imprinted Large-Area Nanopatterned Antireflection Coating, *Nano Letters* 15 (2015) 4223–4228.

[49] S. S. Latthe, C. Terashima, K. Nakata, A. Fujishima, Superhydrophobic Surfaces Developed by Mimicking Hierarchical Surface Morphology of Lotus Leaf, *Mole-cules* 19 (2014) 4256–4283.

[50] B. Bhushan, Y. C. Jung, Natural and biomimetic artificial surfaces for superhydro-phobicity, self-cleaning, low adhesion, and drag reduction, *Progress in Materials Science* 56 (2011) 1–108.

[51] P. Roach, N. J. Shirtcliffe, M. I. Newton, Progess in superhydrophobic surface development, *Soft Matter* 4 (2008) 224–240.

[52] V. Zorba, E. Stratakis, M. Barberoglou, E. Spanakis, P. Tzanetakis, S. H. Anastasiadis, C. Fotakis, Biomimetic Artificial Surfaces Quantitatively Reproduce the Water Repellency of a Lotus Leaf, *Advanced Materials* 20 (2008) 4049–4054.

[53] M. Miwa, A. Nakajima, A. Fujishima, K. Hashimoto, T. Watanabe, Effects of the surface roughness on sliding angles of water droplets on superhydrophobic surfaces, *Langmuir* 16 (2000) 5754–5760.

[54] Y. Y. Yan, N. Gao, W. Barthlott, Mimicking natural superhydrophobic surfaces and grasping the wetting process: A review on recent progress in preparing superhydrophobic surfaces, *Advances in Colloid and Interface Science* 169 (2011) 80–105.

[55] A. Marmur, Wetting on hydrophobic rough surfaces: To be heterogeneous or not to be?, *Langmuir* 19 (2003) 8343–8348.

[56] N. A. Patankar, Transition between superhydrophobic states on rough surfaces, *Langmuir* 20 (2004) 7097–7102.

[57] H. S. Dhowre, S. Rajput, N. A. Russell, M. Zelzer, Responsive cell-material interfaces, *Nanomedicine* 10 (2015) 849–871.

[58] A. Curtis, C. Wilkinson, Topographical control of cells, *Biomaterials* 18 (1997) 1573–1583.

[59] M. T. Frey, I. Y. Tsai, T. P. Russell, S. K. Hanks, Y. L. Wang, Cellular responses to substrate topography: Role of myosin II and focal adhesion kinase, *Biophysical Journal* 90 (2006) 3774–3782.

[60] T. Yeung, P. C. Georges, L. A. Flanagan, B. Marg, M. Ortiz, M. Funaki, N. Zahir, W. Y. Ming, V. Weaver, P. A. Janmey, Effects of substrate stiffness on cell morphology, cytoskeletal structure, and adhesion, *Cell Motility and the Cytoskeleton* 60 (2005) 24–34.

[61] M. Tirrell, E. Kokkoli, M. Biesalski, The role of surface science in bioengineered materials, *Surface Science* 500 (2002) 61–83.

[62] Y. Yang, K. W. Leong, Nanoscale surfacing for regenerative medicine, *WIREs Nanomedicine and Nanobiotechnology* 2 (2010) 478–495.

[63] S. Verma, A. J. Domb, N. Kumar, Nanomaterials for regenerative medicine, *Nanomedicine* 6 (2011) 157–181.

[64] A. Sebastian, F. Syed, D. Perry, V. Balamurugan, J. Colthurst, I. H. Chaudhry, A. Bayat, Acceleration of cutaneous healing by electrical stimulation: Degenerate electrical waveform down-regulates inflammation, up-regulates angiogenesis and advances remodeling in temporal punch biopsies in a human volunteer study, *Wound Repair and Regeneration* 19 (2011) 693–708.

[65] P. Reemann, T. Kangur, M. Pook, M. Paalo, L. Nurmis, I. Kink, O. Porosaar, K. Kingo, E. Vasar, S. Kõks, V. Jaks, M. Järvekulg, Fibroblast growth on micro- and nanopatterned surfaces prepared by a novel sol-gel phase separation method, *Journal of materials science. Materials in medicine* 24 (2013) 783–792.

[66] S. Smitha, P. Shajesh, P. Mukundan, K. G. K. Warrier, Sol-gel synthesis of biocompatible silica-chitosan hybrids and hydrophobic coatings, *Journal of Materials Research* 23 (2008) 2053–2060.

[67] J.-H. Lee, H.-E. Kim, K.-H. Shin, Y.-H. Koh, Electrodeposition of biodegradable sol-gel derived silica onto nanoporous TiO2 surface formed on Ti substrate, *Materials Letters* 65 (2011) 1519–1521.

[68] J. M. Brown, E. J. Swindle, N. M. Kushnir-Sukhov, A. Holian, D. D. Metcalfe, Silica-directed mast cell activation is enhanced by scavenger receptors, *American Journal of Respiratory Cell and Molecular Biology* 36 (2007) 43–52.

[69] R. F. S. Lenza, W. L. Vasconcelos, J. R. Jones, L. L. Hench, Surface-modified 3D scaffolds for tissue engineering, *Journal of Materials Science-Materials in Medicine* 13 (2002) 837–842.

[70] S. F. Wang, X. H. Wang, F. G. Draenert, O. Albert, H. C. Schroder, V. Mailander, G. Mitov, W. E. G. Muller, Bioactive and biodegradable silica biomaterial for bone regeneration, *Bone* 67 (2014) 292–304.

[71] K. Kornicka, B. Babiarczuk, J. Krzak, K. Marycz, The effect of a sol-gel derived silica coating doped with vitamin E on oxidative stress and senescence of human adipose-derived mesenchymal stem cells (AMSCs), *Rsc Advances* 6 (2016) 29524–29537.

[72] Y. Y. Li, B. B. Li, G. Xu, Z. S. Ahmad, Z. H. Ren, Y. Dong, X. J. Li, W. J. Weng, G. R. Han, A feasible approach toward bioactive glass nanofibers with tunable protein release kinetics for bone scaffolds, *Colloids and Surfaces B – Biointerfaces* 122 (2014) 785–791.

[73] R. A. Martin, S. Yue, J. V. Hanna, P. D. Lee, R. J. Newport, M. E. Smith, J. R. Jones, Characterizing the hierarchical structures of bioactive sol-gel silicate glass and hybrid scaffolds for bone regeneration, *Philosophical Transactions of the Royal Society A – Mathematical Physical and Engineering Sciences* 370 (2012) 1422–1443.

[74] X. D. Wang, K. S. Rabe, I. Ahmed, C. M. Niemeyer, Multifunctional Silica Nanoparticles for Covalent Immobilization of Highly Sensitive Proteins, *Advanced Materials* 27 (2015) 7945–7950.

[75] J. R. Jones, L. L. Hench, Regeneration of trabecular bone using porous ceramics, *Current Opinion in Solid State & Materials Science* 7 (2003) 301–307.

[76] G. Frenzer, W. F. Maier, Amorphous porous mixed oxides: Sol-gel ways to a highly versatile class of materials and catalysts, Annual Review of Materials Research, City, 2006, pp. 281–331.

[77] S. Balaji, Y. Djaoued, A. S. Albert, R. Bruning, N. Beaudoin, J. Robichaud, Porous orthorhombic tungsten oxide thin films: synthesis, characterization, and application in electrochromic and photochromic devices, *Journal of Materials Chemistry* 21 (2011) 3940–3948.

[78] G. Hayase, K. Kanamori, A. Maeno, H. Kaji, K. Nakanishi, Dynamic spring-back behavior in evaporative drying of polymethylsilsesquioxane monolithic gels for low-density transparent thermal superinsulators, *Journal of Non-Crystalline Solids* 434 (2016) 115–119.

[79] N. J. Shirtcliffe, G. McHale, M. I. Newton, C. C. Perry, Intrinsically superhydrophobic organosilica sol-gel foams, *Langmuir* 19 (2003) 5626–5631.

[80] Y. Tokudome, K. Fujita, K. Nakanishi, K. Miura, K. Hirao, Synthesis of monolithic Al2O3 with well-defined macropores and mesostructured skeletons via the sol-gel process accompanied by phase separation, *Chemistry of Materials* 19 (2007) 3393–3398.

[81] A. Feinle, M. S. Elsaesser, N. Husing, Sol-gel synthesis of monolithic materials with hierarchical porosity, *Chemical Society Reviews* 45 (2016) 3377–3399.

[82] A. Imhof, D. J. Pine, Ordered macroporous materials by emulsion templating, *Nature* 389 (1997) 948–951.

[83] M. A. Alves-Rosa, L. Martins, S. H. Pulcinelli, C. V. Santilli, Design of micro-structure of zirconia foams from the emulsion template properties, *Soft Matter* 9 (2013) 550–558.

[84] F. Carn, A. Colin, M. F. Achard, H. Deleuze, E. Sellier, M. Birot, R. Backov, Inorganic monoliths hierarchically textured via concentrated direct emulsion and micellar template, *Journal of Materials Chemistry* 14 (2004) 1370–1376.

[85] F. Carn, A. Colin, M. F. Achard, H. Deleuze, C. Sanchez, R. Backov, Anatase and rutile TiO2 macrocellular foams: Air-liquid foaming sol-gel process towards controlling cell sizes, morphologies, and topologies, *Advanced Materials* 17 (2005) 62–66.

[86] M. D. Coelho, M. M. Pereira, Sol-gel synthesis of bioactive glass scaffolds for tissue engineering: Effect of surfactant type and concentration, *Journal of Biomedical Materials Research Part B – Applied Biomaterials* 75B (2005) 451–456.

[87] E. P. Santos, C. V. Santilli, S. H. Pulcinelli, Effect of aging on the stability of ceramic foams prepared by thermostimulated sol-gel process, *Journal of Sol-Gel Science and Technology* 26 (2003) 165–169.

[88] G. T. Chandrappa, N. Steunou, J. Livage, Macroporous crystalline vanadium oxide foam, *Nature* 416 (2002) 702–702.

[89] G. T. Vuong, S. Kaliaguine, T. O. Do, A strategy towards macroporous sponge-like networks of metal oxide-surfactant mesophases and bulk metal oxides, *Journal of Porous Materials* 15 (2008) 679–683.

[90] M. Tang, A. Karma, Surface Modes of Coherent Spinodal Decomposition, *Physical Review Letters* 108 (2012) 265701.

[91] V. Russo, L. Protasova, R. Turco, M. de Croon, V. Hessel, E. Santacesaria, Hydrogen Peroxide Decomposition on Manganese Oxide Supported Catalyst: From Batch Reactor to Continuous Microreactor, *Industrial & Engineering Chemistry Research* 52 (2013) 7668–7676.

[92] M. Timusk, A. Kuus, K. Utt, T. Kangur, A. Šutka, M. Järvekülg, M. Knite, Thick silica foam films through combined catalytic decomposition of H_2O_2 and sol–gel processes, *Materials and Design* 111 (2016) 80–87.

[93] M. H. Choi, S. M. Paek, Synthesis and Characterization of New Macroporous SnO2 Foams, *Bulletin of the Korean Chemical Society* 34 (2013) 1388–1390.

[94] A. Loot, L. Dolgov, S. Pikker, R. Lõhmus, I. Sildos, Goniometric Setup for Plasmonic Measurements and Characterization of Optical Coatings, in. O. Fesenko, L. Yatsenko and M. Brodin (Eds.) Nanomaterials Imaging Techniques, Surface Studies, and Applications, Springer New York, City, 2013, pp. 119–134.

[95] T. Kangur, L. Nurmis, M. Järvekülg, Influence of some system parameters on silica surface patterns by sol-gel phase separation method, *IOP Conference Series: Materials Science and Engineering* 49 (2013) 012035.

[96] H. L. Khor, Y. Kuan, H. Kukula, K. Tamada, W. Knoll, M. Moeller, D. W. Hutmacher, Response of cells on surface-induced nanopatterns: Fibroblasts and mesenchymal progenitor cells, *Biomacromolecules* 8 (2007) 1530–1540.

[97] W. L. Min, B. Jiang, P. Jiang, Bioinspired Self-Cleaning Antireflection Coatings, *Advanced Materials* 20 (2008) 3914.

[98] K. Siimon, P. Reemann, A. Põder, M. Pook, T. Kangur, K. Kingo, V. Jaks, U. Mäeorg, M. Järvekülg, Effect of glucose content on thermally cross-linked fibrous gelatin scaffolds for tissue engineering, *Materials Science & Engineering C – Materials for Biological Applications* 42 (2014) 538–545.

ACKNOWLEDGEMENTS

First of all, I would like to thank my supervisors Martin Järvekülg, Valter Kiisk and Ants Lõhmus for their help and support throughout my PhD studies. I am grateful to my colleagues Martin Timusk, Ardi Loot, Fredrik Punga, Rando Saar and former students Liis Nurmis and Agnes Kuus for the help with different experiments and measurements. I would like to acknowledge Paula Reemann, Viljar Jaks and Martin Pook from the interdisciplinary working group for cell growth studies. Finally, I would like to send my regards to my materials science coursemates, group of Imaginaarkuivikud and dear friends for keeping up my motivation when needed.

PUBLICATIONS

CURRICULUM VITAE

Name: Triin Kangur
Date of birth: October 6, 1987
Nationality: Estonian
E-mail: kangur@ut.ee

Education:
2009–2011 University of Tartu, MSc in materials science
2006–2009 University of Tartu, BSc in materials science
2003–2006 Pärnu Koidula Gymnasium
1994–2003 Pärnu Ülejõe Gymnasium

Career:
2012–   University of Tartu, Institute of Physics, specialist
2015–2016 Estonian Materials Technologies Competence Centre, research engineer
2008–2009 University of Tartu, Institute of Physics, laboratory assistant

List of publications:

1. **T. Kangur**, V. Kiisk, A. Loot, M. Timusk, M. Järvekülg, Optical functionality of micro- and nanostructured silica surfaces prepared by a sol-gel phase separation method, *Thin Solid Films* 622 (2017) 11–16.

2. M. Timusk, A. Kuus, K. Utt, **T. Kangur**, A. Šutka, M. Järvekülg, M. Knite, Thick silica foam films through combined catalytic decomposition of H_2O_2 and sol-gel processes, *Materials and Design* 111 (2016) 80–87.

3. M. Klaas, **T. Kangur**, J. Viil, K. Mäemets-Allas, A. Minajeva, K. Vadi, M. Antsov, N. Lapidus, M. Järvekülg, V. Jaks, The alterations in the extracellular matrix composition guide the repair of damaged liver tissue, *Scientific Reports* 6 (2016) 27398.

4. K. Siimon, P. Reemann, A. Põder, M. Pook, **T. Kangur**, K. Kingo, V. Jaks, U. Mäeorg, M. Järvekülg, Effect of glucose content on thermally cross-linked fibrous gelatin scaffolds for tissue engineering, *Materials Science and Engineering C* 42, (2014) 538−545.

5. **T. Kangur**, L. Nurmis, M. Järvekülg, Influence of some system parameters on silica surface patterns by sol-gel phase separation method, *IOP Conference Series: Materials Science and Engineering* 49 (2013) 012035.

6. P. Reemann, **T. Kangur**, M. Pook, M. Paalo, L. Nurmis, I. Kink, O. Porosaar, K. Kingo, E. Vasar, S. Kõks, V. Jaks, M. Järvekülg, Fibroblast growth on micro- and nanopatterned surfaces prepared by a novel sol-gel phase separation method, *Journal of Materials Science: Materials in Medicine* 24 (2013) 783–792.

7. M. Järvekülg, R. Välbe, J. Jõgi, A. Salundi, **T. Kangur**, V. Reedo, J. Kalda, U. Mäeorg, A. Lõhmus, A.E. Romanov, A sol-gel approach to self-formation

of microtubular structures from metal alkoxide gel films, *Physica Status Solidi A – Applications and Materials Science*, 209 (2012) 2481–2486.

8. V. Kiisk, **T. Kangur**, M. Paalo, T. Tätte, S. Lange, S. Pikker, I. Sildos, Structural and luminescence characteristics of SnO_2:Eu and SnO_2:Eu,Sb nanophosphors upon annealing at high temperatures, *Materials Chemistry and Physics* 130 (2011) 293–298.

ELULOOKIRJELDUS

Nimi: Triin Kangur
Sünniaeg: 6. oktoober, 1987
Kodakondsus: Eesti
E-post: kangur@ut.ee

Haridus:
2009–2011   Tartu Ülikool, Tehnikateaduste magister (materjaliteadus)
2006–2009   Tartu Ülikool, Tehnikateaduste bakalaureus (materjaliteadus)
2003–2006   Pärnu Koidula Gümnaasium
1994–2003   Pärnu Ülejõe Gümnaasium

Töökogemus:
2012–   Tartu Ülikool, Füüsika Instituut, spetsialist
2015–2016   Eesti Materjalitehnoloogiate Arenduskeskus, insener
2008–2009   Tartu Ülikool, Füüsika Instituut, laborant

Publikatsioonide loetelu:

1. **T. Kangur**, V. Kiisk, A. Loot, M. Timusk, M. Järvekülg, Optical functionality of micro- and nanostructured silica surfaces prepared by a sol-gel phase separation method, *Thin Solid Films* 622 (2017) 11–16.
2. M. Timusk, A. Kuus, K. Utt, **T. Kangur**, A. Šutka, M. Järvekülg, M. Knite, Thick silica foam films through combined catalytic decomposition of H_2O_2 and sol-gel processes, *Materials and Design* 111 (2016) 80–87.
3. M. Klaas, **T. Kangur**, J. Viil, K. Mäemets-Allas, A. Minajeva, K. Vadi, M. Antsov, N. Lapidus, M. Järvekülg,V. Jaks, The alterations in the extracellular matrix composition guide the repair of damaged liver tissue, *Scientific Reports* 6 (2016) 27398.
4. K. Siimon, P. Reemann, A. Põder, M. Pook**, T. Kangur**, K. Kingo, V. Jaks, U. Mäeorg, M. Järvekülg, Effect of glucose content on thermally cross-linked fibrous gelatin scaffolds for tissue engineering, *Materials Science and Engineering C* 42, (2014) 538–545.
5. **T. Kangur**, L. Nurmis, M. Järvekülg, Influence of some system parameters on silica surface patterns by sol-gel phase separation method, *IOP Conference Series: Materials Science and Engineering* 49 (2013) 012035.
6. P. Reemann, **T. Kangur**, M. Pook, M. Paalo, L. Nurmis, I. Kink, O. Porosaar, K. Kingo, E. Vasar, S. Kõks, V. Jaks, M. Järvekülg, Fibroblast growth on micro- and nanopatterned surfaces prepared by a novel sol-gel phase separation method, *Journal of Materials Science: Materials in Medicine* 24 (2013) 783–792.
7. M. Järvekülg, R. Välbe, J. Jõgi, A. Salundi, **T. Kangur**, V. Reedo, J. Kalda, U. Mäeorg, A. Lõhmus, A.E. Romanov, A sol-gel approach to self-formation

of microtubular structures from metal alkoxide gel films, *Physica Status Solidi A – Applications and Materials Science*, 209 (2012) 2481–2486.

8. V. Kiisk, **T. Kangur**, M. Paalo, T. Tätte, S. Lange, S. Pikker, I. Sildos, Structural and luminescence characteristics of SnO_2:Eu and SnO_2:Eu,Sb nanophosphors upon annealing at high temperatures, *Materials Chemistry and Physics* 130 (2011) 293–298.

DISSERTATIONES SCIENTIAE MATERIALIS
UNIVERSITATIS TARTUENSIS

1. **Martin Järvekülg.** Tubular microstructures by Hf-, Zr- and Ti-butoxide gel sheet rolling. Tartu, 2011, 112 p.
2. **Sergei Vlassov.** Investigation of nanoscale interactions and mechanical properties of nanostructures using quartz tuning fork based real-time measurements. Tartu, 2011, 171 p.
3. **Margus Kodu.** Pulsed Laser Deposition of Magnesium Oxide and Barium Ternary Oxides for Plasma Display Protective Layers. Tartu, 2011, 89 p.
4. **Rainer Pärna.** Surface studies of some oxide films. Tartu, 2011, 129 p.
5. **Jevgeni Šulga**. Self-assembly and interaction of nanostructures. Tartu, 2011, 114 p.
6. **Wojciech Kuznik.** Quantum-chemical computer simulations of the linear and non-linear optical properties of pyrazoloquinoline and dicyanopyrazine derivatives. Tartu, 2012, 89 p.
7. **Leonid Dorogin.** Structural and tribological properties of zero- and one-dimensional nanocrystals. Tartu, 2012, 193 p.
8. **Viljar Palmre.** Fabrication and characterization of microporous carbon-based electroactive polymer actuators. Tartu, 2012, 99 p.
9. **Madis Paalo**. Synthesis of CNT-metal oxide nanocomposites: sol-gel process, rheology, structural and functional properties. Tartu, 2014, 175 p.
10. **Raul Välbe.** Developement of ionic liquid composites by sol-gel method for elaboration of industrial nano- and microstructures. Tartu, 2014, 97 p.
11. **Urmas Joost.** Impurity and preparation dependent properties of titania thin films. Tartu, 2014, 155 p.
12. **Madis Umalas**. Application of sol-gel technology for production of ceramic nanocomposites and functional coatings. Tartu, 2015, 136 p.
13. **Elena Samsonova.** Energy transfer probe as a tool to study morphological and structural origins of fluorescence quenching in rare-earth doped nanophosphors. Tartu, 2015, 114 p.
14. **Jay Mondal.** Novel Corrosion Protective Nanostructured Composite Coatings. Tartu, 2016, 104 p.
15. **Kathriin Utt.** Metal oxide mesostructures for optical applications. Tartu, 2016, 88 p.
16. **Kaido Siimon.** Electrospun gelatin cross-linked by glucose. Tartu, 2016, 84 p.
17. **Marko Part.** Combined three-dimensional sol-gel structures and atomic layer deposited thin films. Tartu, 2017, 162 p.
18. **Pejman Rasti.** Analysis of Remote Sensing Image Super Resolution using Fluid Lenses. Tartu, 2017, 188 p.
19. **Ivo Romet.** Recombination luminescence of doped borates: origin and application prospects in dosimetry. Tartu, 2017, 111 p.

20. **Vladimir I. Kondratiev.** Processing and characterization of transparent electrode materials. Tartu, 2017, 111 p.
21. **Taivo Jõgiaas**. Mechanical properties of atomic layer deposited thin films and nanocomposites. Tartu, 2017, 125 p.
22. **Lauri Aarik**. Atomic layer deposition and characterization of thin oxide films for application in protective coatings. Tartu, 2017, 180 p.